Light transmission through subwavelength slits

A needle's eye problem

BACHELOR RESEARCH PROJECT PHYSICS

Johannes Simon

Supervisor: Dr. E.R. Eliel

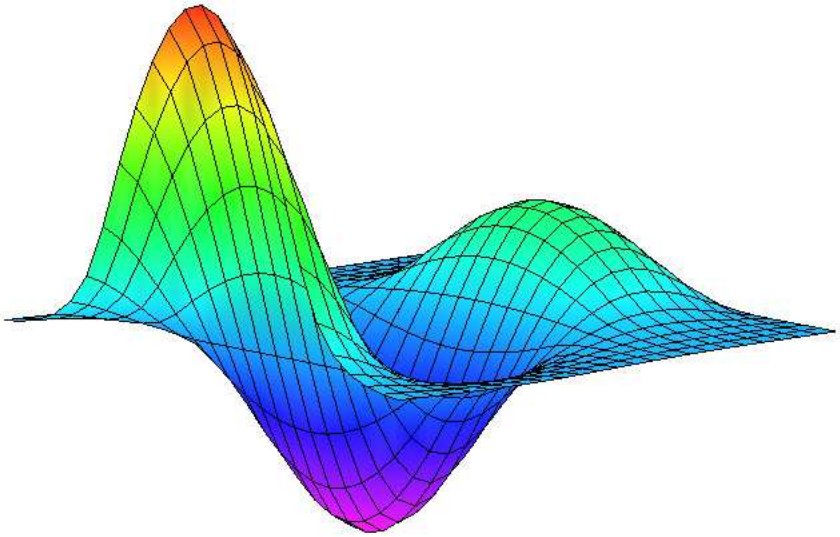

June 4, 2009

The title page shows a three-dimensional plot of the amplitude of the electric field's y-component for TE-polarized light with a wavelength of 400 nm in a 200 nm wide slit in a gold film. The width of the slit is in the x-direction and the x-dependence of the field resembles a Gaussian. Along the length of the slit (i.e., the thickness of the metal film) the wave propagates, but is damped. The film's thickness is here modeled to be five times that of the actual sample in the experiments to better show the attenuation effect of a traveling wave in a slit aperture.

Abstract

The polarization dependent transmission properties of a slit aperture in a thin gold layer were measured for light with different wavelength.
TE-polarized light was found to be transmitted equally well as the TM-polarized component up to twice the expected cutoff wavelength of the slit. At longer wavelength the relative transmission of the TE-polarization does weaken. For light that is a linear combination of TE and TM (we used light polarized at 45° with respect to the slit axis) this results in a change of the angle of the output polarization.
To understand these dichroic properties of the slits a theoretical model was derived to explain the transmission in terms of a waveguide picture including the loss of TM-polarized light due to excitation of surface plasmon waves at the slit edges.

Contents

1 Introduction

Understanding the interaction of light with very small physical structures is essential to many fields of technology, like optical computing and optical data storage. These small structures are interesting because of the wish for miniaturization of components and because they open new ways of light manipulation [1].
In this thesis I will describe the results of a study of the transmission of normally incident light through sub-wavelength slits and derive a model that describes the interaction between light with varying wavelength and polarization, and the slit to explain the experimental results.
The slit structure under study will be a double-slit with a separation of 25 μm between the slits. Each slit is 50 μm high and 200 nm wide and they are milled into a 200 nm thick gold film. The fact that double-slit structures are studied instead of single slits is simply due to the fact that I wanted to use an existing sample instead of waiting for a new one (with single slits) to be made. The shape anisotropy of the slits should give them dichroic properties since different polarizations of incident light will be confronted with different boundary conditions.

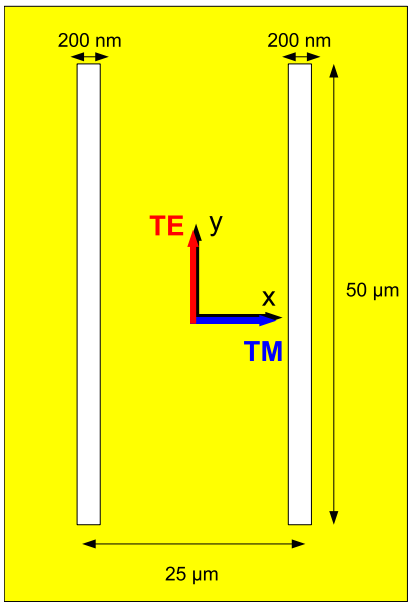

Figure 1: The dimensions of the double-slit structure used in the experiment. The polarization of incident light can be split in two orthogonal components, which transmit through the slits differently. The TE- or transverse electric component is the component of the electric field vector that is parallel to the long axis of the slits while for the TM- or transverse magnetic component the electric field is perpendicular to the slits.

The wavelength of the light in the experiments (500 - 1500 nm) is longer than the perfect-metal cutoff wavelength ($\approx$ 400 nm) for these apertures. This should result in strong attenuation of the TE-polarization, i.e., the polarization that has its electric field parallel to the slits long axis. Therefore, for incident light with an arbitrary polarization, the transmitted light will have different polarization properties as compared to the incident light.
My interest for this study was raised, because experiments by N.V. Kuzmin [2] suggested that the transmission of the attenuated TE-polarization through such slits is much higher than one would expect from a waveguide picture. Kuzmin used a single wavelength of light and variable slit width's in his experiments and he identified the ratio of the wavelength of the light and the width of the slit as the relevant parameter. My supervisor and I were interested to see whether this is still so when we use different wavelengths of light for which the refractive index of gold varies.

There are three main contributions that will be evaluated to give an explanation of the transmission properties of a metallic slit:

1. A single slit is modeled as a waveguide with boundary conditions corresponding to those of a real metal wall.
2. Back and forth scattering of the wave along the optical axis of the waveguide is treated as a Fabry-Pérot interference.
3. Excitation of surface plasmons explaining the weakening of the transmitted transverse magnetic polarization (TM).

The first contribution (the waveguide picture) will be discussed in great detail in this thesis while the other two are treated more qualitatively due to the limited scope of the research project.

2 Theory

In this section I will discuss the physics that is required to understand the experiment that has been conducted.

2.1 Waveguide picture of a slit aperture

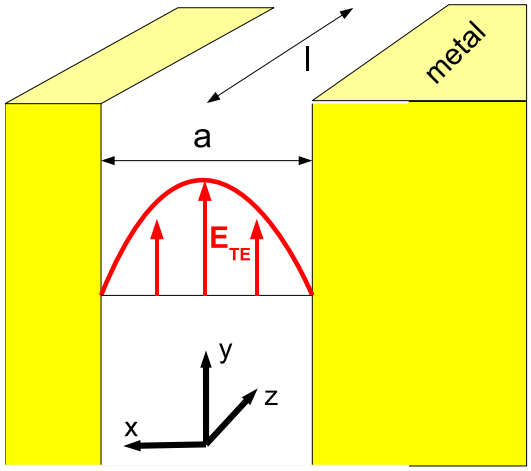

Figure 2: The spatial distribution of the y-component of the electric field of the TE-mode. In a waveguide picture it has to form a standing wave in the x-direction to fulfill the boundary conditions. In the z-direction we expect an exponential decay of the wave's amplitude. In this image the waves don't penetrate the surrounding metal, as it is supposed to be an ideal conductor.

A simplified picture of a slit in a metal layer is that of a waveguide, where the thickness of the layer is the length of the waveguide. If such a waveguide is made of an ideal metal, then the electric field parallel to the surface will go to zero at the boundary between air and metal, because the ideal conductor can neutralize the field by unlimited induced currents [6]. Because the light waves have to have a node at the boundaries, they are forced to form standing waves between the opposing metal walls of the waveguide. Consequently an integer multiple of half the wavelength λ_x of this standing wave has to fit in the waveguide's width a

$$a = n \cdot \lambda_x/2;\ n \in \mathbb{N}. \tag{1}$$

Because the waveguide extends much further along y than along x, we will treat it as if it extends infinitely in the y-direction. Figure 2 illustrates the distribution of the electric field of the transverse electric (TE) mode within the waveguide; it consists only of the y-component of the incident electric field. The transverse magnetic (TM) mode - given by the y-component of the magnetic field - has its magnetic field parallel to the slit (and the electric field perpendicular) and will not be quantized since we assume an infinitely high slit. So, as a result of the shape of the aperture, the TE- and TM-mode will transmit differently. The field components E_y (TE) and H_y (TM) are chosen because, in this type of rectangular waveguides, together they suffice to describe the complete fields via Maxwell's equations (Eq. (7)) and because their distribution in the x-direction is easily derived using the boundary conditions as we will see in Section 2.2.

First, let us get a general overview of the mechanism by which the standing wave condition for the TE-mode affects its propagation and eventually leads to its attenuation. We should remember, that the wavelength of light is related to its momentum p by

$$p = \hbar k = h/\lambda. \tag{2}$$

In this equation $k = |\vec{k}| = 2\pi/\lambda$ is the wave-number and $h = 2\pi\hbar$ is Planck's constant. To form waves between the slit's walls, momentum has to be transferred from the incident lights z-component to the x-component of the standing wave through scattering of the incident wave at the edges of the slit. Because of the symmetry of the scattering edges equal momentum is created in the x- and the $-x$-direction, resulting in standing waves (Fig. 3).

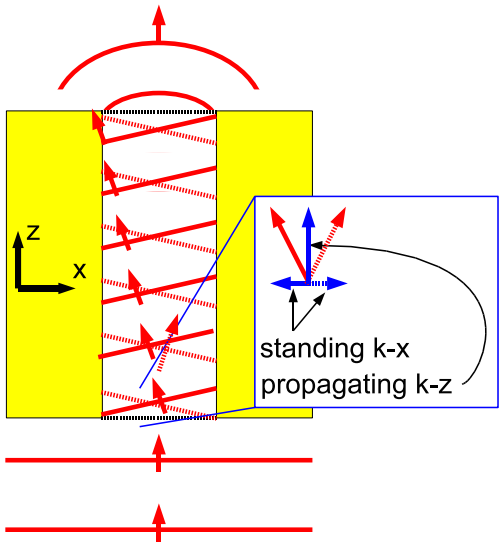

Figure 3: To create the standing waves, some momentum in the x-direction has to be borrowed from the z-component of the k-vector. One interpretation is, that because the total vector $\vec{k}$ stands orthogonal on the wavefronts, that the light bounces back and forth in the waveguide.

The components of $\vec{k}$ obey the following rules:

$$\vec{k} = k_x\hat{x} + k_y\hat{y} + k_z\hat{z}, \tag{3}$$
$$k^2 = k_x^2 + k_y^2 + k_z^2. \tag{4}$$

The free-space wave-vector $\vec{k}_{vac}$ of the incident light in our coordinate system only has a z-component, its length is given by the color, i.e., the wavelength of the light. If this length of the total wave vector is smaller than the minimum $k_x = 2\pi/\lambda_x$ for a standing wave, it follows from Eq. (4) that the z-component of $\vec{k}$ will be imaginary in the waveguide, resulting in exponential damping of the wave.

So the maximum wavelength of incident light that can pass through the slits - called the cutoff wavelength - is $\lambda_{co} = 2a$ or twice the width of the waveguide. This means, that for the TE-mode the cutoff wavelength in the experiment is 400 nm. For the TM-mode there is no such cutoff in the limit of an infinitely high waveguide, but even with the real height of 50 μm, this cutoff is still at 100 μm. So we expect TE polarized light to be strongly attenuated, while the TM-mode passes through the aperture unhindered, at the wavelengths that were used in the experiments.
This picture of a idealized waveguide needs some refinement to be applicable to a slit aperture in a thin metal film. If the z-component of the TE-wave-vector becomes imaginary within the slit, this does not necessarily mean that no light is transmitted - it means that the electric and magnetic field amplitudes of the mode will decrease exponentially along the length of the waveguide (z-direction). So if the metal film is thin enough a considerable amount of light may be transmitted. Furthermore, the electric and magnetic fields can penetrate slightly into the metal, because we are not dealing with an ideal conductor. This effectively increases the cutoff wavelength of the slit as the electric field in the TE-mode does not need to go zero at the boundaries.
These two points which both increase TE-transmission will be addressed in the following section.

2.2 Real waveguides

In reality, even above the cutoff wavelength a considerable amount of light is transmitted through such slits [2]. It will take a closer look into the electrodynamics of the light-metal interaction, to explain this. The derivation of the waveguide modes, that I give here, essentially follows the work of O.T.A. Janssen [3].

All classical electromagnetic phenomena can be described by Maxwell's equations:

$$\begin{aligned} \nabla \times \vec{H} &= \epsilon \partial \vec{E}/\partial t + \vec{J}, & (5)\\ \nabla \times \vec{E} &= -\mu \partial \vec{H}/\partial t, & (6)\\ \nabla \cdot \vec{J} &= -\partial \rho/\partial t. & (7) \end{aligned}$$

Here $\vec{H}$ and $\vec{E}$ stand for the magnetic and the electric field, while $\vec{J}$ and ρ are the current density and the electric charge density, respectively. The parameters ϵ and μ are the electric permittivity and the magnetic permeability, both of which are material properties which depend on the frequency ω of the oscillating fields.
We do not have any external sources of current in any of the media present in our experiment. So the only electric current that we have to deal with is induced by the alternating electric field $\vec{E}$ via the relation $\vec{J} = \sigma(\omega) \cdot \vec{E}$, with σ the wavelength-dependent conductivity of the metal. Since none of our media is magnetic, μ is equal to the constant vacuum permeability μ_0.
For light the electric and magnetic fields take the form of harmonic waves. Both fields are real vector fields. However calculations will be more convenient when we treat them as complex fields:

$$\begin{aligned} \vec{E}(r,t) &= \vec{E}(r) \cdot e^{-i\omega t} = \vec{E_0} \cdot e^{i\vec{k}\cdot\vec{r}} \cdot e^{-i\omega t}, & (8)\\ \vec{H}(r,t) &= \vec{H}(r) \cdot e^{-i\omega t} = \vec{H_0} \cdot e^{i\vec{k}\cdot\vec{r}} \cdot e^{-i\omega t}. & (9)\\ & & (10) \end{aligned}$$

Substituting this into Maxwell's equations results in the following relations between the spatial parts of the fields:

$$\begin{aligned} \nabla \times \vec{H} &= -\imath\omega\epsilon\vec{E} + \vec{J} = (-\imath\omega\epsilon + \sigma)\vec{E} = -\imath\omega\tilde{\epsilon}\vec{E}, & (11)\\ \nabla \times \vec{E} &= \imath\omega\mu_0\vec{H}, & (12) \end{aligned}$$

where $\tilde{\epsilon}$ is a complex permittivity defined as:

$$\tilde{\epsilon} = \epsilon + \imath\sigma/\omega. \quad (13)$$

It is easy to see from Eqs. (11) and (12) that, within an ideal metal where σ would be infinitely large, the field amplitudes are zero. A real metal however will not be able to exclude the electric and magnetic field completely because of ohmic losses in the material. This property can be expressed as a complex refractive index $n = \sqrt{\tilde{\epsilon}}$ of the metal, which tells us, how an electromagnetic wave gets refracted and attenuated in the metal [4]. The refractive index, like the permittivity, depends on the wavelength of the light. For slow changing electric fields and currents, i.e. a long wavelength of the incident light, the metal will behave very much like an ideal conductor. For short wavelengths however, it gets increasingly difficult for the electrons to follow the driven oscillations due to their inertia; consequently the electric field can penetrate the metal.

The boundary conditions at the surface of a real metal with normal vector $\hat{n}$ are

$$\hat{n} \times (\vec{H}_2 - \vec{H}_1) = 0, \tag{14}$$
$$\hat{n} \times (\vec{E}_2 - \vec{E}_1) = 0, \tag{15}$$

where the indices 1 and 2 are referring to the fields in the waveguide and in the metal walls, respectively. This means that the components of $\vec{E}$ and $\vec{H}$ parallel to the metal are continuous at the interface, a fact that we will enable us to find their spatial distribution in the x-direction (,i.e. the width of the slit).

As I stated earlier, within the air gap of the slit we will have a standing wave in the x-direction with a real wave number k_x. In the gold walls on the other hand we will have an exponential attenuation of the standing wave, represented by a imaginary wave number $k_{(x,Au)}$. For an E- or H-field pointing in the y-direction (,i.e. along the height of the slit,) the components of $\vec{k}$ are related to each other by

$$k_x^2 + k_z^2 = k_0^2 \text{ (in the slit)}, \tag{16}$$
$$k_{(x,Au)}^2 + k_z^2 = k_0^2 n_{Au}^2 = k_0^2 \tilde{\epsilon}_{Au} \text{ (in the metal)}, \tag{17}$$

because of conservation of momentum (Eqs. (2) - (4)). The component k_z does not change at the air-metal interface inside the slit because there is no symmetry breaking in the z-direction, but only in the x-direction. Consequently Eqs. (16) and (17) yield

$$k_{(x,Au)} = \sqrt{k_0^2(\tilde{\epsilon}_{Au} - 1) + k_x^2}. \tag{18}$$

I will first derive a solution for the TE-mode, by matching the standing and evanescent parts of the electric field at the boundary. Because of the symmetry of the waveguide the solutions for the electric field will also be symmetric

$$E_y(x,z) = E_y(x) \cdot e^{\imath k_z z} : \tag{19}$$
$$E_y(x) = \begin{cases} Be^{-\imath k_{(x,Au)} x} & (x \leq -a/2), \\ A\{e^{\imath k_x x} + e^{-\imath k_x x}\} & (-a/2 \leq x \leq a/2), \\ Be^{\imath k_{(x,Au)} x} & (x \geq +a/2). \end{cases} \tag{20}$$

Applying the continuity conditions for the parallel field components (Eq. (14) and (15)) and one of the reduced Maxwell equations (Eq. (12)) yields the following set of equations:

$$Be^{\imath k_{(x,Au)} a/2} = A\{e^{\imath k_x a/2} + e^{-\imath k_x a/2}\}, \tag{21}$$
$$k_{(x,Au)} Be^{\imath k_{(x,Au)} a/2} = \pm k_x A\{e^{\imath k_x a/2} - e^{-\imath k_x a/2}\}. \tag{22}$$

Equation (22) follows from Eq. (12) and (21) and represents H_z (the magnetic field in the z-direction); the plus sign on the right-hand-side corresponds to the boundary $x = a/2$ and the minus sign to $x = -a/2$.
Substitution of Eq. (21) in Eq. (22) gives

$$\begin{pmatrix} (k_{(x,Au)} + k_x)e^{-\imath k_{(x,Au)} a/2} & (k_{(x,Au)} - k_x)e^{\imath k_{(x,Au)} a/2} \\ (k_{(x,Au)} - k_x)e^{\imath k_{(x,Au)} a/2} & (k_{(x,Au)} + k_x)e^{-\imath k_{(x,Au)} a/2} \end{pmatrix} \cdot \begin{pmatrix} A \\ B \end{pmatrix} = \vec{0}, \tag{23}$$

which is solvable only if the determinant of the matrix is zero, because only then the amplitudes A and B can be unequal to zero. This is equivalent to the requirement

$$e^{\imath k_x a} = \pm \frac{k_x + k_{(x,Au)}}{k_x - k_{(x,Au)}}, \tag{24}$$

where the plus sign corresponds to symmetric modes, in which we are interested here because of the symmetric boundary conditions. Substituting Eq. (18) for $k_{(x,Au)}$ we can now solve this numerically or graphically (Fig. 4) and thereby find k_x for the TE-mode.
For the TM-mode we use H_y as our starting point and get, by analogous treatment of the matching conditions,

$$e^{\imath k_x a} = \pm \frac{\tilde{\epsilon}_{Au} k_x + k_{(x,Au)}}{\tilde{\epsilon}_{Au} k_x - k_{(x,Au)}}. \tag{25}$$

Given k_x we can, using Eq. (17), calculate the z-component k_z of the wave vector in the slit. The knowledge of the complex wave vector (see Fig. 5) allows us to compute the spatial distribution of the E- and H-field anywhere in the slit. In Figs. 6 and 7 the real and imaginary part of the electric field in TE-mode and the magnetic field in the TM-mode are plotted, respectively, for a wavelength $\lambda = 500$ nm.
Figures 8 to 10 illustrate the physical implications that arise from the difference in wave vectors of the modes. Relevant for transmission is especially that the TE-mode has a decay length that converges to a finite value - so there will always be some TE-transmission - and that the TM-mode is almost unaffected by the slit.
The imaginary part of the refractive index of gold ($n_{Au} = \sqrt{\tilde{\epsilon}_{Au}}$) gets larger for increasing wavelengths of light and because of $k_{Au} = k_0 n_{Au}$, this translates into an exponential decay of the harmonic wave ($e^{\imath \vec{k}_{Au} \vec{r}}$) and the field will penetrate less into the walls. In Fig. 11 to 13 some examples of the instantaneous field-distributions are plotted for illustration purposes.

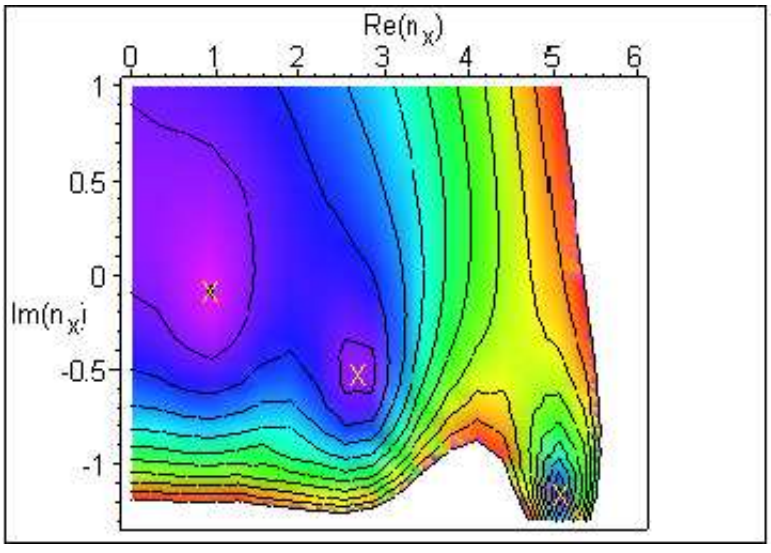

Figure 4: Graphical solution of Eq. (24): The allowed values of k_x can be found by subtracting the right-hand side from the left-hand side and looking for its roots (for plotting purposes I chose the absolute value of this function, which includes the same roots). The figure actually shows the x-component of the effective refractive index $n_x = k_x/k_0$ within the slit for an incident wavelength of 500 nm. The yellow X's mark the value of n_x found by solving Eq. (24) numerically. The solution with the smallest real value corresponds to the mode of longest wavelength for the standing wave between the slit walls. I used this for further calculations, since this "ground state" should be dominant in the TE-mode. The imaginary part of the solutions for n_x are all negative (see Fig. 5). Colors in the plot indicate function values between 0 (purple) and 20 (red) - higher function values are in white.

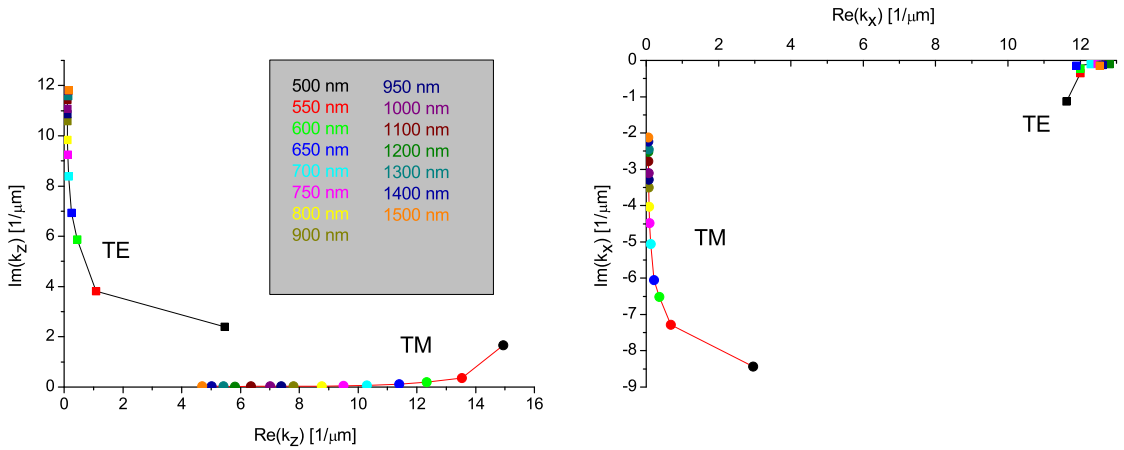

Figure 5: The z- and x-components of the wave vector for the TE- and TM-modes are plotted in the complex plane for the wavelengths of the incident light used in the experiment. In the limit of long wavelengths k_z gets almost completely imaginary for the TE-mode, corresponding to a pure exponential decay of $E_y(z)$, while at shorter wavelengths the real part is still producing some spatial oscillation corresponding to a traveling wave. For the TM-mode k_z becomes completely real as wavelength increases and the gold film acts more like an ideal metal (see Figs. 9 and 10). The wave vector's x-component is almost completely real for the TE-mode and corresponds to a standing wavelength of ≈ 500 nm - 20% more than the theoretical cutoff wavelength. The TM-mode in turn has a highly negative imaginary part, resulting in a hyperbolic cosine shape of $H_y(x)$ (see Fig. 7).

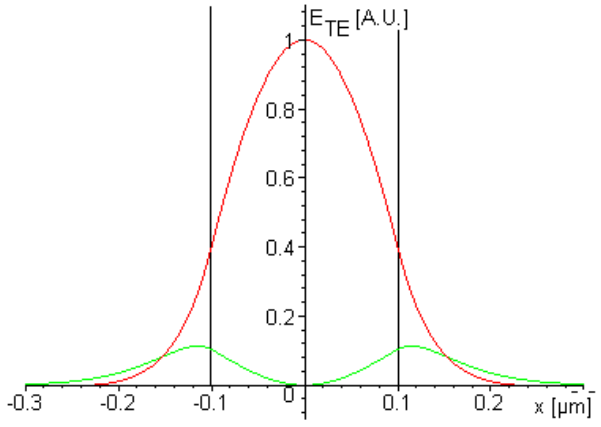

Figure 6: For a TE-mode ($\lambda = 500$ nm) we find the shape of the E-field (E_y) between the walls from the x-component of the wave vector (red $\equiv$ Re(E_y), green $\equiv$ Im(E_y)). As we would expect the real part of the field has a cosine shape in the slit and an exponential decay in the walls.

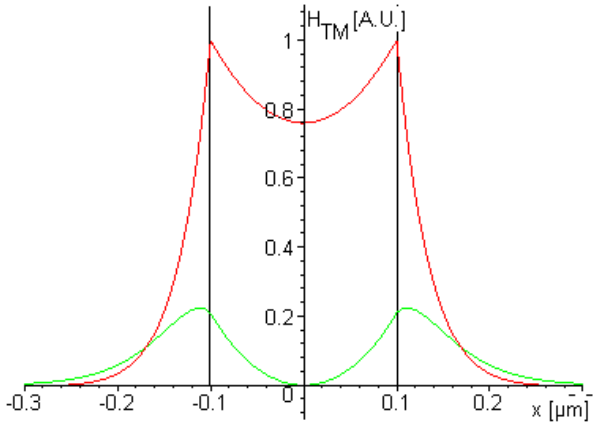

Figure 7: The H-field in the TM-mode (red $\equiv$ Re(H_y), green $\equiv$ Im(H_y), $\lambda = 500$ nm) has a rather unexpected shape. Because of the negative imaginary component of k_x the field increases exponentially with distance from the center of the slit until we reach the wall, while the cosine associated with the very small real part of k_x is essentially constant over the width of the slit. Within the wall we have then again an exponential decay.

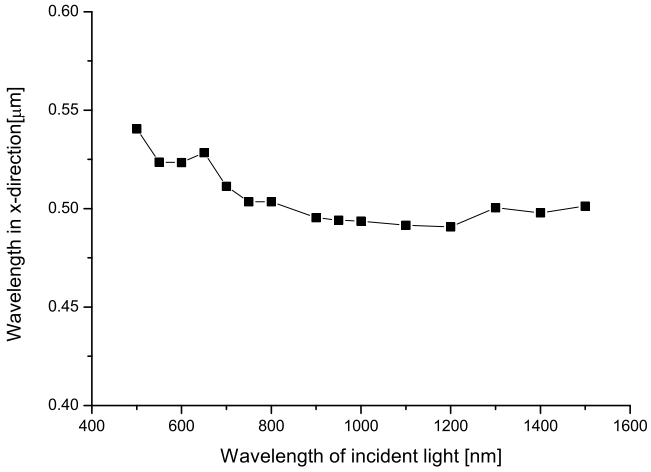

Figure 8: The wavelength of the standing wave within the slit, associated with the real component of k_x, is plotted for the TE-mode, to give an idea of the effective cutoff wavelength of the slit. The values of k_x were calculated using Eq. (24) for a slit modeled after the sample used in the experiments. If the slit was cut into an ideal metal the wavelength in x-direction would be just 400 nm for the TE-mode. Here however penetration of the fields into the walls of the slit results in standing waves of $\approx 20\%$ greater length. The jumps at 650 and 1300 nm can be traced back to irregularities in the table of the refractive indices used in the calculations (Table 1, [4]).

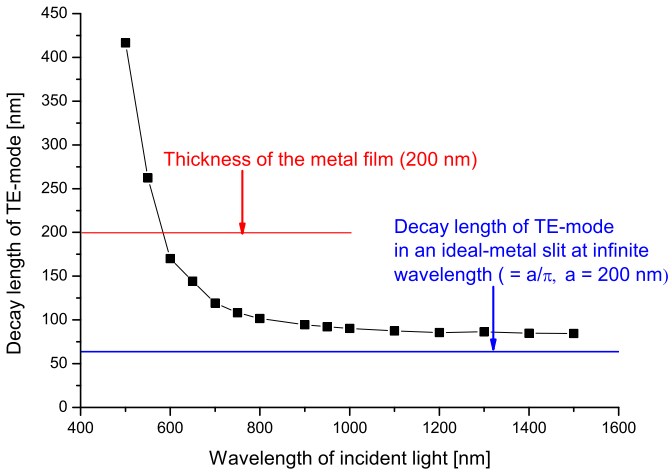

Figure 9: Decay length of the TE-wave along the slit: After we know the complex x-component k_x of the wave vector we can calculate its z-component using Eq. (16). The imaginary part k_z gives us the decay length of the mode in the slit (i.e., the length after which the amplitude of the field has decreased by a factor e). It is a measure of the attenuation of the wave. The blue line gives the value to which the decay length L_{dec} converges at longer wavelengths, where the gold film acts as an ideal metal. It is given by the relation $L_{dec}^{-1} = \mathrm{Im}k_z = \mathrm{Im}\sqrt{k_0^2 - k_x^2}$, where $k_x = 2\pi/\lambda = \pi/a$. So $L_{dec} \to a/\pi$ for $\lambda \to \infty$.

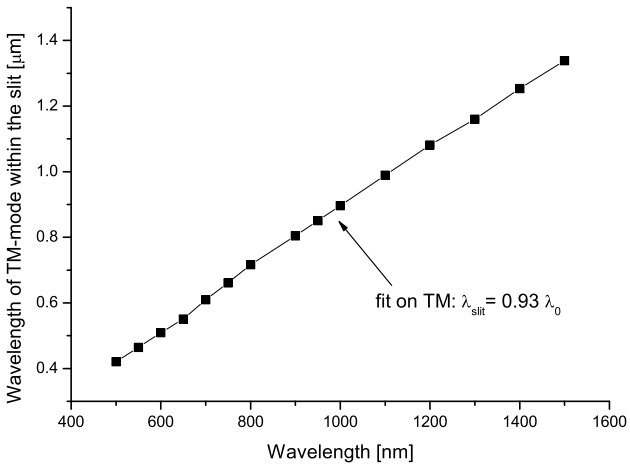

Figure 10: Wavelength within the slit: The wavelength of the TM-mode (associated with its almost completely real k_z) is very close to that of the free wave and increases linearly with it (see linear fit value in figure). This is a further indication, that the slit is essentially transparent to the TM-mode.

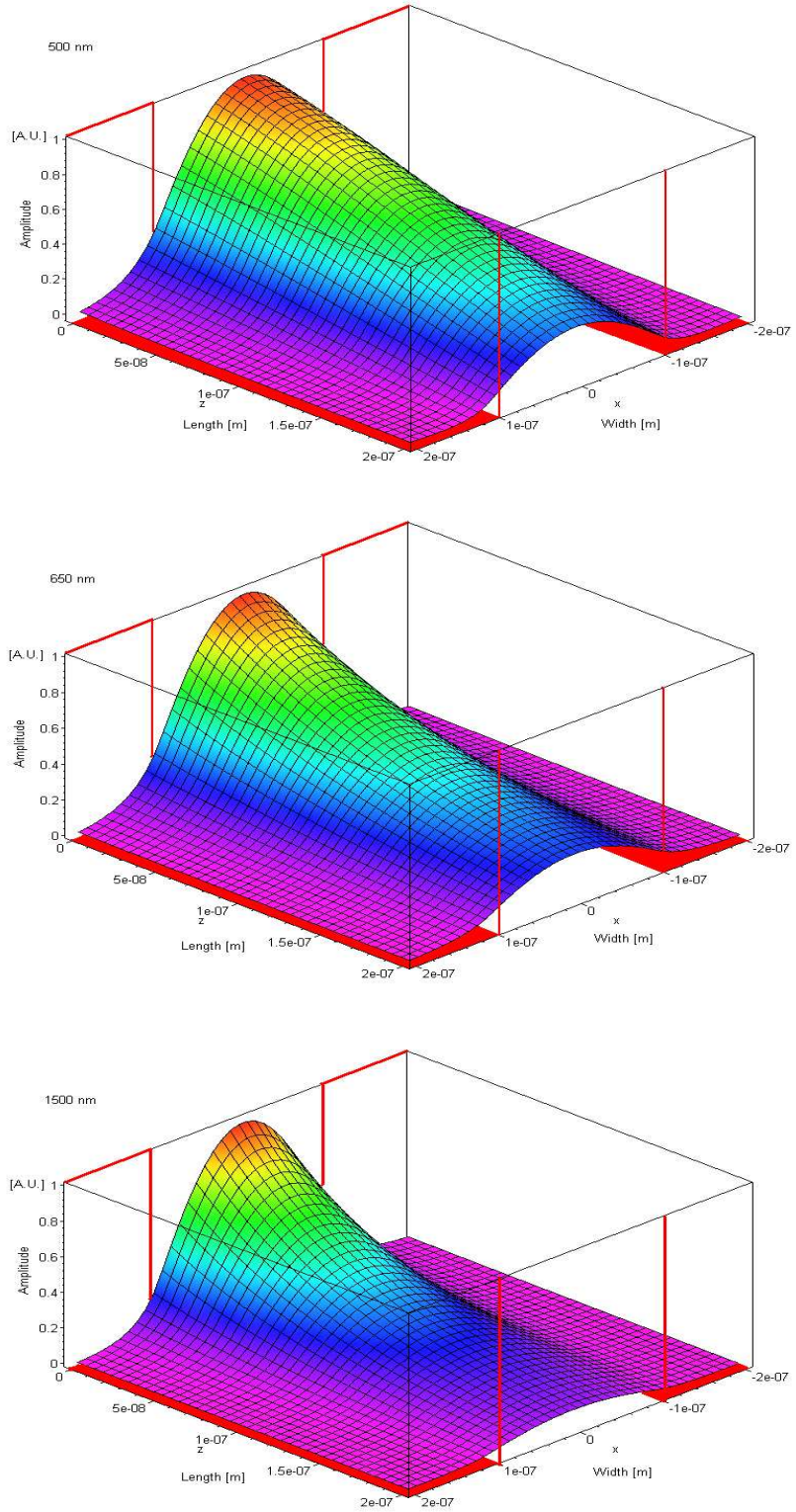

Figure 11: Instantaneous amplitude of TE-polarized electric field within the waveguide for a wavelength of 500, 650 and 1500 nm, respectively. The refractive index of gold (Table 1) has been used to characterize the material response of the waveguide. The values of the k-vectors where calculated by solving Eq. (24). Values on the x- and z-axis are in meters and the amplitude of the field is normalized with respect to the free-space field. One can clearly see that the transmitted amplitude decreases with wavelength. At 500 nm the wave still oscillates in the waveguide, i.e., it is not yet (over-)critically damped. One can see this from the fact that in the z-direction the contour of the function is still convex. But even much further above the cutoff wavelength the amplitude does not completely decay within the waveguide and a considerable amount of light is transmitted. The slit boundaries are indicated by red lines at $x = \pm 100$ nm.

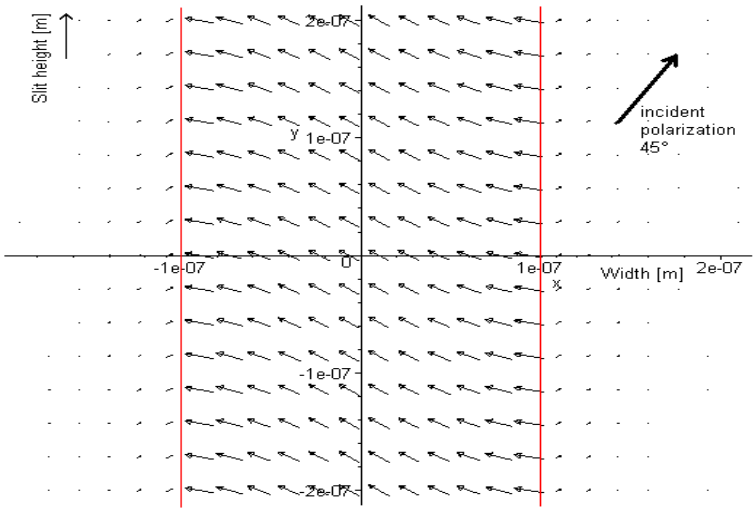

Figure 12: Configuration of the instantaneous electric field (TE- plus TM-component) in the exit plane of the slit ($z = 200$ nm, time $t = 0$ s, $\lambda_{in} = 500$ nm). Notice, that only the field component parallel to the slit is continuous at the boundary ($x = \pm 100$ nm, indicated by red vertical line). The perpendicular component changes sign because of the negative real part of the permittivity of the metal. The apparent turn of the polarization axis results from the different propagation constants of the two modes within the slit.

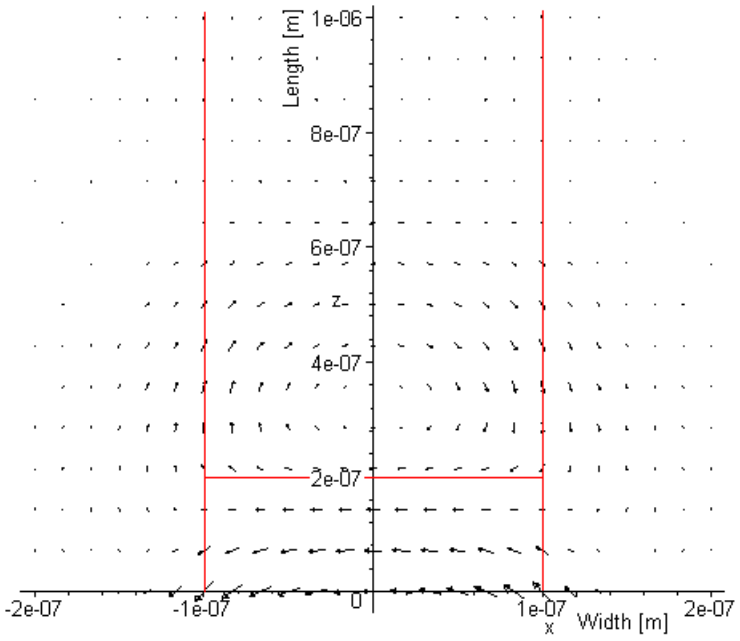

Figure 13: Plot of the instantaneous magnetic field distribution of the TE-mode along the length z of the slit (time $t = 0$ s, $\lambda_{in} = 500$ nm). Because $\vec{E} \propto \nabla \times \vec{H}$ there is also a component of H_{TE} in the z-direction. It is clearly visible how the magnetic field curls around the electric field which points into the page ($\hat{y}$) in the TE-mode. Note, that in our experiment the slit ends already at $z = 200$ nm.

2.3 Fabry-Pérot interference

When light strikes an interface between two media with different refractive indices, part of it is reflected due to the impedance mismatch of the media and part is transmitted. The reflection and

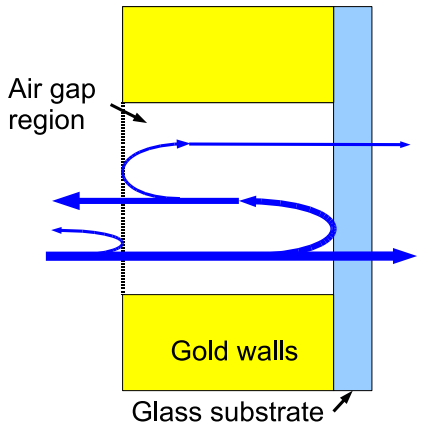

Figure 14: Fabry-Pérot interference: Light is partially reflected at boundaries where the refractive index changes. If it bounces back and forth it can interfere with the light that is initially transmitted. Relative to this it has a phase difference, that is introduced both due to the extra path length and because each reflection gives an additional phase jump. This figure only pictures the Fabry-Pérot interference inside the slit, however we must expect that the glass substrate will also generate a Fabry-Pérot interference (see text below).

transmission of polarized light that hits such an interface is determined by the effective refractive indices in the direction of travel ($n_z = k_z/k_0$) of the two media. We can always decompose an EM-wave into two component with either the electric or the magnetic field vector parallel to the interface (TE- and TM-components), just like we did already for the modes in our waveguide. Here the TE- and TM-components are the same polarizations as in the description of the waveguide, because a field-component that is parallel to the slit walls is also parallel to the front- and back-plane of the slit's opening: In the TE-case the electric field only has a y-component, while the magnetic field has both an x- and a z-component. In the TM-case it is vice versa.

The transmission and reflection coefficients t and r are given by the Fresnel equations [5] and can be brought into the convenient form

$$r_{TE} = r_{TM} = (-)\frac{k_{z1} - k_{z2}}{k_{z1} + k_{z2}} = (-)\frac{n_{z1} - n_{z2}}{n_{z1} + n_{z2}} \tag{26}$$

$$t_{TE} = t_{TM} = \frac{k_{z1}}{k_{z1} + k_{z2}} = \frac{n_{z1}}{n_{z1} + n_{z2}}, \tag{27}$$

, where the indices 1 and 2 refer two the incident and the transmitting medium, respectively. The minus sign in Eq. (26) is associated with the TM-mode reflection coefficient. Although the form of the reflection and transmission coefficients is essentially the same for both modes, their k_z-components are of course different within the slit.
To first order the transmission process can be described in 3 steps:

1. Transmission from air to the slit
2. Guided wave in the slit
3. Transmission from slit to glass substrate.

Put into an equation this looks as follows:

$$t_0 = t_{air\to slit} \cdot e^{\imath k_z l} \cdot t_{slit\to glass} = t_{as} e^{\imath k_z l} t_{sg} \tag{28}$$

where l is the length of the waveguide, i.e., the thickness of the gold film. Each of the three factors in this equation gives a different contribution for the TE- and TM-mode. Light that is not transmitted to the glass is reflected back into the slit. If this light reflects at the front from the slit-air interface we get an additional contribution to the transmission. This gives the series

$$1 + r_{sg} e^{2\imath k_0 n_z l} r_{sa} + (r_{sg} e^{2\imath k_0 n_z l} r_{sa})^2 + ... = 1/(1 - r_{sg} e^{2\imath k_0 n_z l} r_{sa}) \tag{29}$$

for the multiple reflections that will contribute to transmission, resulting in Fabry-Pérot interference. The product of Eqs. (28) and (29) then gives us the complex transmission coefficient for the waveguide

$$t_{total} = \frac{t_{as} e^{\imath k_0 n_z l} t_{sg}}{(1 - r_{sg} e^{2\imath k_0 n_z l} r_{sa})}. \tag{30}$$

Its absolute value carries the transmitted field-amplitudes in it, while its complex phase represents the overall phase-shift of the transmitted wave.
Because the gold film is much thinner than the wavelength of the light, it might be that Fabry-Pérot interference does only slightly affect the transmission of the slit.
Although Fabry-Pérot interference in the glass substrate is probably not negligible (due to the high reflectivity of the metal film), I will not include it in the model for the following reason: The interference should give the same contribution for the TE- and TM-mode as they behave the same in the glass medium and because I will eventually look at the ratio of the TE- and TM-transmission, the effects of Fabry-Pérot interference in the substrate should cancel each other.

2.4 Surface plasmon excitation

Surface plasmons (SP) are electromagnetic disturbances that travel along the interface between a good conductor[1] and a dielectric. The electric field extends into both materials, where its strength decreases exponentially. What is interesting in the context of the slit transmission that we study is, that plasmons can be generated by the TM-component of incoming light, but not by the TE-component [2].

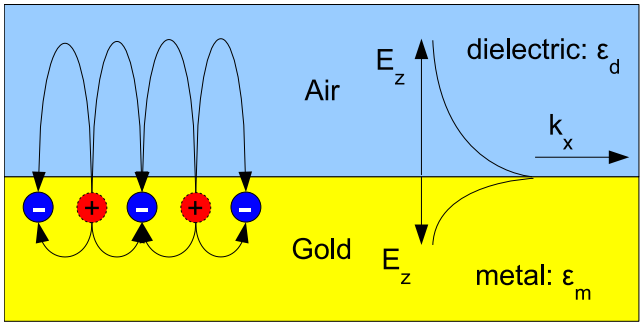

Figure 15: Plasmon propagation: The electric field spans between the oscillating negative and fixed positive charges. The field-amplitude decreases exponentially with the distance from the interface. The field moves as a wave with wave-number k_x.

Part of the TM-polarized light will be converted to SPs and travel along the surface in both directions away from the slit. While it travels, an SP weakens due to ohmic loss. If it encounters a second slit on its way, it has a chance of becoming a photon again and being radiated through that slit or in the

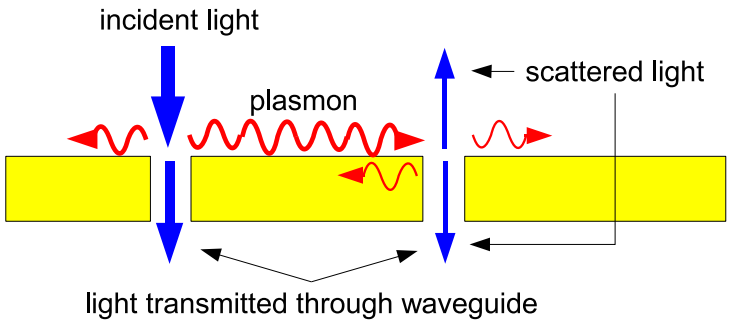

Figure 16: Scattering of surface plasmons: At sharp edges light and SP can couple and transfer energy. A portion of that SP can radiate light into the second slit.

opposite direction (Fig. 16). So via the path light→plasmon→light we get light that interferes with the directly transmitted light. More importantly there is a portion of the TM-light that will not pass through the slits at all, resulting in a higher *relative* transmission of the TE-polarization.
How large a fraction of the TM-polarization will be converted to SPs and thereby lost for transmission? I will give a simplified description in which the TM-mode is only weakened due to plasmon excitation. Thereby I neglect all other scattering effects at the slit which might also weaken the transmitted TM-component. Also the plasmon generation itself will be treated rather qualitatively due to the complexity of the problem.
Surface plasmons cannot spawn directly from light because of a momentum mismatch. Additional momentum has to be "generated" by surface features. These can "generate" momentum proportional to the square of the Fourier transform of their physical shape ($\vec{r} - space \rightarrow \vec{k} - space$) [2]. Remember, that this also happened at the edges of a waveguide and the "generation" of momentum is really a deflection or scattering of the light.
The probability P to excite a plasmons at a certain wave number k_x is proportional to the squared fourier transform FT of the slit's shape

$$P \propto (\mathsf{FT}(a))^2 = [\frac{\sin(k_{xSP} \cdot a/2)}{k_{xSP}/2}]^2, \tag{31}$$

where a is the width of the slit [2, 7, 8]. As a simplified model I will here use

$$P = \alpha \cdot [\frac{\sin(k_{xSP} \cdot a/2)}{k_{xSP}/2}]^2, \tag{32}$$

where α is just a proportionality constant, while in reality it still varies with the wavelength of incident light [7]. It will later be used as a fitting parameter, when comparing the measured data with the model. The wave number of the plasmons that are generated is furthermore related to the free space wave number $k_0 = 2\pi/\lambda$ of the light by

$$k_{xSP} \quad = \quad \mathsf{Re}(k_0 \sqrt{\frac{n_{Au}^2(\lambda)}{1 + n_{Au}^2(\lambda)}}). \tag{33}$$

So there is just one plasmon wave number excited at a given color of the incident light and Eq. (32) can be evaluated [2].
It is logical to assume that the probability P of creating a plasmon is proportional to the loss in light intensity of the TM-mode: Every photon in an incident TM-polarized beam would have a chance P to be scattered into a plasmon and all its intensity would be lost to transmission. So the intensity of the TM-light that enters the slit would be reduced to $1 - P$ times the incident intensity. With this argumentation I am assuming that there are no other mechanisms involved at the slit entry and

[1]Note: Good conductor here means a metal with low loss at optical frequencies. Examples are gold, silver and aluminium.

exit, which treat the two polarizations differently. A more complete and quantitative analysis of SP-excitation is given by P. Lalanne et al. [9].

Furthermore, in the case of a double-slit, as used in the experiments, plasmons can reradiate light at the second slit, which leads to interference. I will give a short description of this phenomenon at the end of Section 4.

3 Experiment

In this section I will describe the setup and sample that I used in the experiment. I will also explain how I collected data and what those data look like.

3.1 Sample

The sample houses 15 horizontal double-slits with a length of 50 μm. The width of a slit is either $0.2, 0.4$ or 0.6 μm and their separation equals $5, 10, 15, 20$ and 25 μm. All these structures were milled with a focussed ion beam into a 200 nm thick gold film, which is evaporated on a 10 nm titanium adhesion layer with fuzed quartz glass as a carrier. In the experiment the slits with width 0.2 μm and separation 25 μm were used. These narrow slits have a theoretical cutoff wavelength of 400 nm. Because I used light between 500 and 1500 nm, I was able to study the transmission properties for wavelengths much larger than the cutoff wavelength.

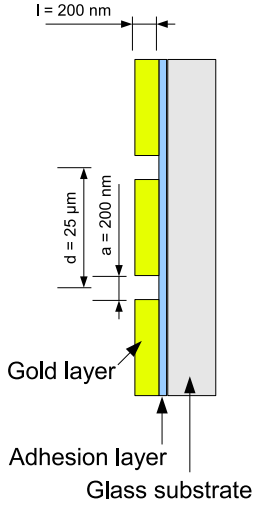

Figure 17: Slit arrangement on sample.

3.2 Setup

To illuminate the sample I used a so-called white light laser (Fianium SC 450-2). A number of narrow bandpass filters were inserted to produce from the white light a beam of nearly monochromatic light at different wavelengths between 500 and 1500 nm. The monochromatic light is polarized at an angle of 45° with respect to the direction of the slits, after which it passes through a focussing lens that makes a light spot of 1–2 mm diameter on the double-slit.
The double slit, like in Young's experiment, produces an interference pattern. Since we are interested in the total transmission of light through the metallic slit structure and not in the interference pattern, the transmitted light is focussed on our sensor.[2] To achieve this, the light is first collimated by a set of lenses and a metal pin is used to block the zeroth order of the interference to get rid of any light that shimmers through the sample. The collimated interference pattern is next sent through a series of slits in a box to block all stray light that might come from anywhere but the double-slit. Finally the light is focussed on the detector. To measure the polarization of the transmitted light a second polarizer is placed as an analyzer in front of the detector. At the transition from visual to infrared

[2]Focussing the light will make all optical paths from slit to detector have the same length, so the relative phases of different maxima are zero at the detector.

right (i.e., $\lambda > 1000$ nm) I switched from a Si-detector to an InGaAs-detector, to make optimal use of their spectral sensitivity. The polarizers used in the setup were both chosen and checked to work well in the visual and the IR regime.
A detailed description of the different components of the setup is given in the appendix.

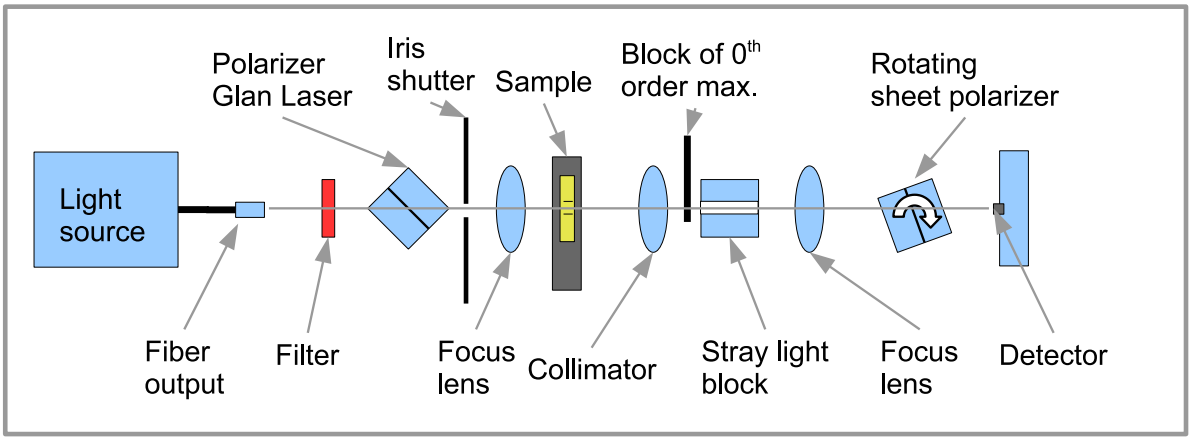

Figure 18: Experimental setup.

3.3 Measurement

3.3.1 Measurement method

The measurement is conducted in darkness. The laser is polarized at 45° with respect to the slits. I measure the voltage output of the sensor, which is proportional to the power or average light intensity that strikes its photodiode. First the voltage is measured while the shutter in front of the sample is closed to get an offset reference for the sensor voltage, which tends to drift over long time scales (a complete measurement run takes ≈ 40 min.). Next I open the shutter and measure the voltage of the illuminated sensor. After turning the analyzer by 10° the whole process is repeated until all 360° are covered.
A computer program was written in LabView to simplify data collection: during each measurement the computer automatically performs 30 read outs of the sensor output and saves the average of these together with their standard deviation and the corresponding analyzer-angle. The standard deviation will be given as error bars in the measured data (Figs. 20 and 21) and used as an inverse weight of each data point, as I fit data in Section 3.3.3. I believe that the main source of the measurement variance is due to fluctuations of the laser output power, which vary from measurement to measurement.

3.3.2 Data

Since the incident light is 100% linearly polarized we expect to obtain a perfectly "8" shaped polar graph in the polarization-dependent transmission when the slit is absent. The form is an 8, because the polarizer lets the fraction $\cos\alpha^2$ of the light intensity pass, where α is the angle between the polarization of the light and the axis of the polarizer.
As the slit is introduced in the setup, the figure 8 is distorted, indicating anisotropic transmission properties of the slit. If the TE- and TM-components of the light were transmitted equally well, then we should get an 8 in the polar graph that has its main axis at 45°. A widening of the 8 indicates elliptically polarized light which results from a phase shift between TE and TM. A rotation of the 8 results as well from a change in the ratio of TE- vs. TM-polarized light and a phase difference between both modes.
Figures 20 and 21 show the results of our measurements at a series of wavelengths. Apparently

the TE- and TM-components of the light get transmitted equally well at wavelength < 1000 nm. As the wavelength increases the TM-component (orthogonal to the slit-direction) becomes dominant. The later fact makes it difficult to give a direct interpretation of the plots in Figs. 20 and 21. For example at wavelengths ≤ 900 nm the 8 figure suggests higher transmission of the TE-mode compared to the TM-mode, while at $\lambda = 1500$ nm the orientation of the 8 at an angle smaller than $0°$ is probably due to a phase difference $> 90°$ between the two modes. To clarify this a more extensive analysis follows in Section 4.

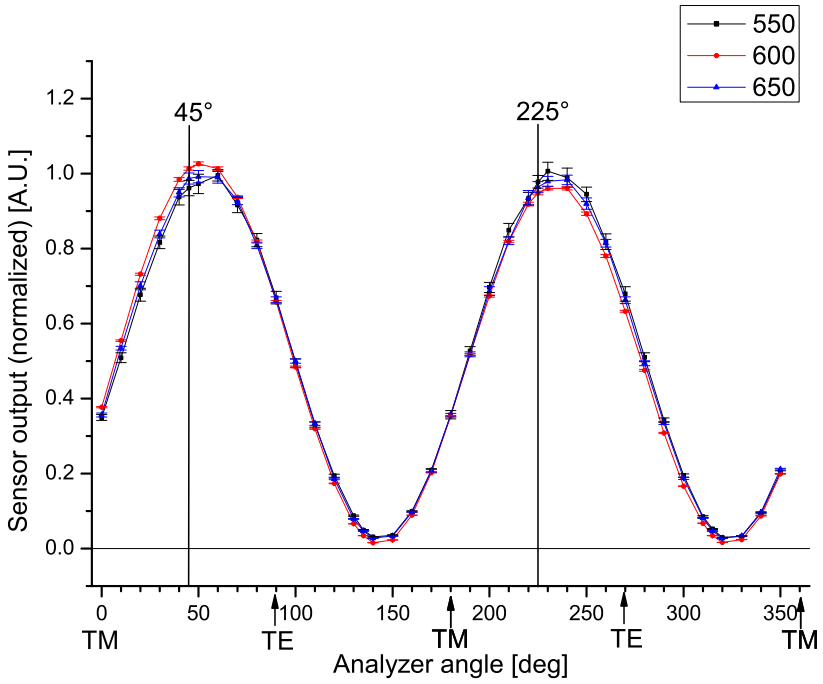

Figure 19: Graphs of the measurement curves at $\lambda = 550$, 600 and 650 nm. The very narrow opening of the figure 8 is better visible here than in corresponding polar plots of Figs. 20 and 21. Because the transmission almost reaches zero at certain angles the light is almost linearly polarized and the angle of polarization (towards TE) can only be the result of stronger transmission of the TE-light compared to TM-light.

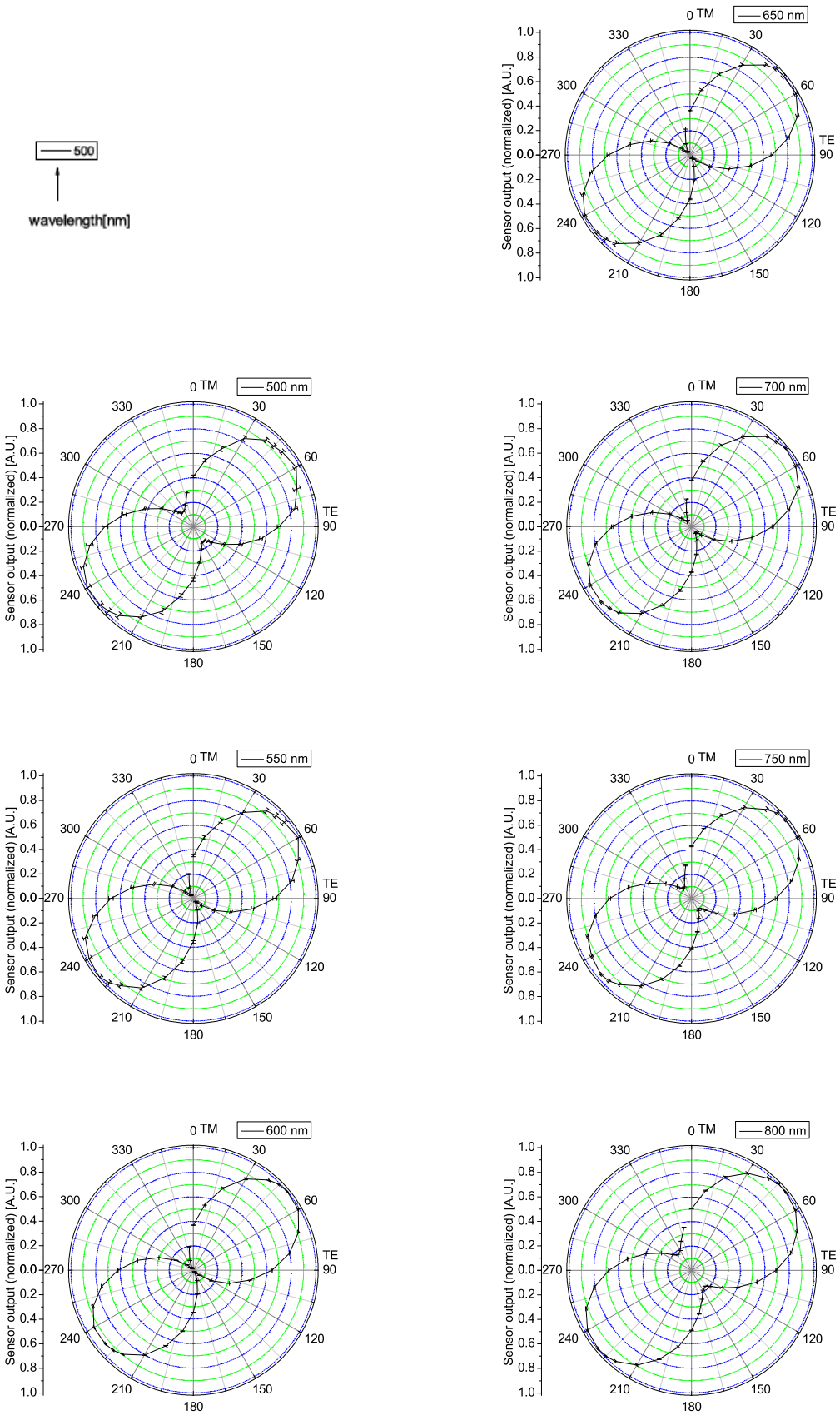

Figure 20: Normalized intensity of transmitted light at different wavelength for different polarizer angles, Part 1 of 2. Incident light is polarized at 45°-angle. Increasing wavelengths are sorted in columns.

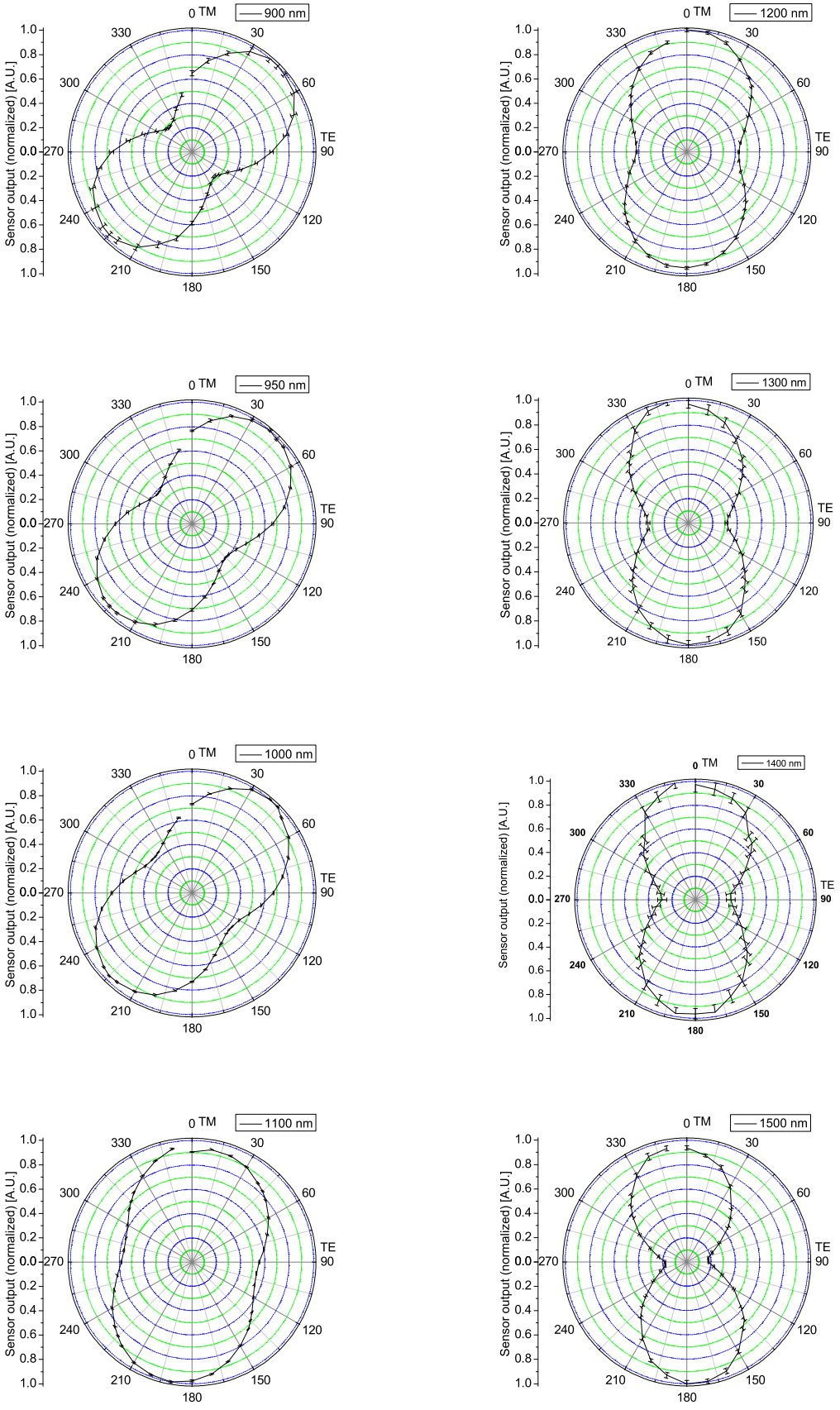

Figure 21: Normalized intensity of transmitted light at different wavelength for different polarizer angles, Part 2 of 2. Data are normalized, because the amount of incident light varies with wavelength.

3.3.3 Change in polarization

The figure 8 shapes in the plots in Figs. 20 and 21 result from the fact, that only the component of the electric field parallel to the analyzer axis is transmitted. For linearly polarized light we get a cosine-squared dependence, which is an "8" in a polar plot. In many of the 8's the intensity does not go to zero at any angle. This offset is due to elliptical polarization of the light (I took great care to eliminate unpolarized stray light, which would also create an offset). Elliptical polarization occurs when the TE- and TM-component acquire a relative phase difference. Elliptically polarized light can be decomposed into a linearly and a circularly polarized component. The circularly polarized light looks the same for any angle of the analyzer and therefore the combination of linear and circular polarization shows an offset in our measurements. I will use the following fit-function to determine the angle of maximum intensity and the offset in the measured data:

$$I := A \cdot cos^2(\pi/180° \cdot (\alpha - \alpha_0)) + B. \tag{34}$$

With α the variable angle of the analyzer and fitting parameters A, α_0 and B being the amplitude of the varying part of the signal, the angle of maximum intensity and the offset, respectively. Fitting all data of Figs. 22 and 23 with Eq. (34) yields values of α_0, A and B.

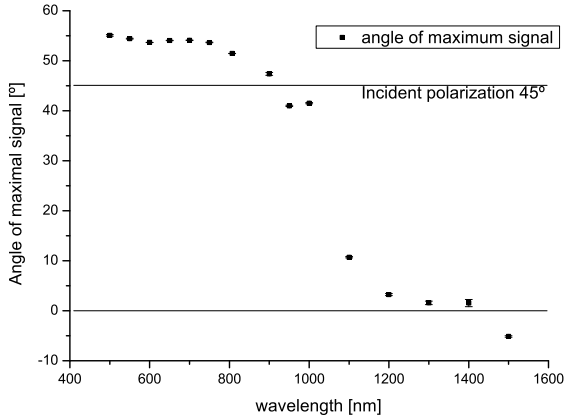

Figure 22: Analyzer angle α_0 for maximum intensity of transmitted light.

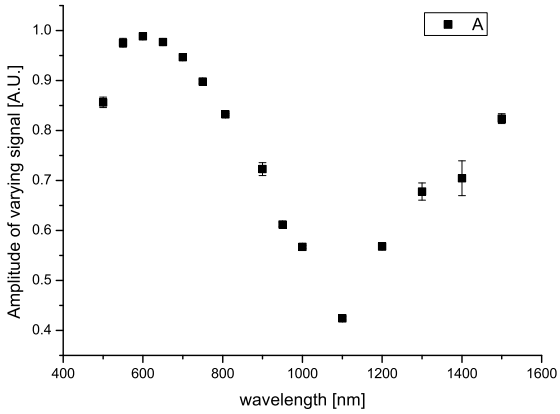

Figure 23: Amplitude A of the varying part of the intensity. Because the total intensity is normalized the offset $B = 1 - A$.

A striking fact is, that for all wavelengths up to 900 nm the TE-mode seems to transmit better than the TM-mode. This is odd, since we initially expected that mode to be attenuated very strongly by the narrow slits. Around $\lambda \approx 1000$ nm - far above the theoretical cutoff wavelength of 400 nm - the angle of maximum intensity changes very rapidly. Why the polarization angle drops under the zero-degree line at $\lambda = 1500$ nm is unclear. It could mean that the phase difference between transmitted TE and TM is larger than 90°.
In order to get a deeper physical understanding of the transmission characteristics of the slit aperture we will however need to extract the TE- and TM-field and their phase difference from the measurements. This will be done in the next section.
These result don't yet give us deeper physical understanding of the polarization dependent transmission properties, but they are nonetheless interesting if one wants to use the slits in an application where one would for example want to translate the wavelength of incident light into an output polarization.

4 Results and discussion

In this section I will determine the polarization-dependent transmission properties of the double slit from the measurement data. Furthermore, I will try to convince you that the different theoretical models from Section 2 provide a qualitative description of these properties.

4.1 Mode decomposition

Of course, changing the angle of the input polarization, which is equivalent to changing the input ratio of TE- and TM-polarized light, would change the output polarization. We can learn much more about the polarization properties of thin slits by directly looking at the TE- and TM-components of the light and determining their attenuation and relative phase difference. The electric field of the light will be written as a vector in the basis $\{TE, TM\}^T$. Because our light source and filters make it difficult to tell how much light is falling onto the sample at any wavelength, it is much more convenient to look at relative differences in the transmission of both components, so we get rid of that difficulty. If C is the amplitude ratio $\frac{|E_{TE}|}{|E_{TM}|}$ and δ is the phase difference between TE and TM, then the transmission matrix of our sample in the basis $\{TE, TM\}^T$ is given by:

$$\mathbf{S} := \begin{bmatrix} C\exp(\imath\delta) & 0 \\ 0 & 1 \end{bmatrix}. \tag{35}$$

The light next passes through our analyzer, whose transmission is described by:

$$\mathbf{P} := \begin{pmatrix} \cos(\alpha) \\ \sin(\alpha) \end{pmatrix}, \tag{36}$$

where α is the analyzer's polarization angle. So the action of the sample and the analyzer on the light can be summarized as

$$\vec{E}_{out} = \mathbf{P}^T\mathbf{S}\vec{E}_{in}. \tag{37}$$

In the case that the incoming polarization is 45° relative to the axis of the slits the electric field of the incoming wave becomes

$$\vec{E}_{in} = \tfrac{E_0}{\sqrt{2}}\begin{pmatrix} 1 \\ 1 \end{pmatrix}. \tag{38}$$

We can now calculate $\vec{E}_{out}$ from this input.
The quantity we measure in an experiment is however the irradiance at the photodiode. The time-averaged irradiance is given by:

$$\begin{aligned} I &= \frac{\epsilon_0 c}{2}|\vec{E}_{out}|^2 \\ &= \frac{\epsilon_0 c}{4}E_0^2\{C^2\cos(\alpha)^2 + \sin(\alpha)^2 + 2C\cdot\cos(\alpha)\sin(\alpha)\cos(\delta)\}. \end{aligned} \tag{39}$$

This expression can now be used as a fit function, a polar plot shows us, that it has indeed the right shape to fit our data (see Fig. 24). The parameters used are $C = 0.5$ and $\delta = \pi/4$ ($\frac{E_0\epsilon_0 c}{4} \equiv 1$) resulting in a polarization-angle of $= 70.5°$ ($TE\hat{=}0°$) after the sample.

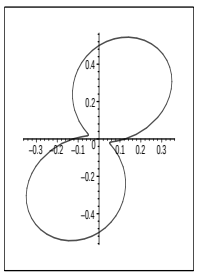

Figure 24: Plot of Eq. (39)

The relative transmission of the TE- and TM-mode (parameter C, see Fig. 25) and the angle of the phase difference between these modes (parameter δ, Fig. 26) are extracted from the data with Eq. (39) as a fit function. We can only find the absolute value of the phase difference, because the equation contains δ in the cosine, so it might actually be that the values for $\lambda < 600$ nm extend into the negative domain.

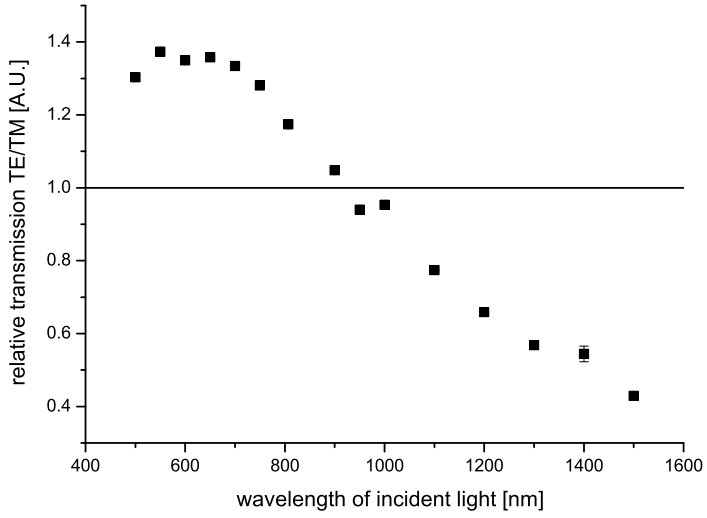

Figure 25: Relative transmission of TE- and TM-polarized mode. The TE-polarized light transmits better than the TM-component at short wavelengths, although we are far above the theoretical cutoff wavelength of 400 nm. Gradually the transmission ratio of the TE-mode vs. TM decreases and only at $\lambda > 900$ nm has the TM-mode a higher transmission.

It is surprising how large the relative transmission of the TE-mode is compared to the TM-mode. Though I would have expected a fast attenuation of this mode as the wavelength of the incident light increases, it actually transmits stronger than the TM-mode up to almost 1000 nm[3]. Even at $\lambda = 1500$ nm the relative transmission of the TE-polarization is still about half of the TM-transmission. This is also surprising because gold acts almost like a perfect conductor for light with long wavelength, meaning that the electric field can hardly penetrate the metal an therefore is even confined more strongly.

The phase difference between the two modes starts at relatively small angles and grows with increasing wavelength. It is not surprising that there is a stronger retardation effect as the

[3]Kuzmin reports that this dominance of the TE-transmission over the TM-transmission at small wavelength to slit width ratios (λ/a) was already discovered by M.H. Fizeau around 1861 and Kuzmin himself did numerical calculations which predict the same [2].

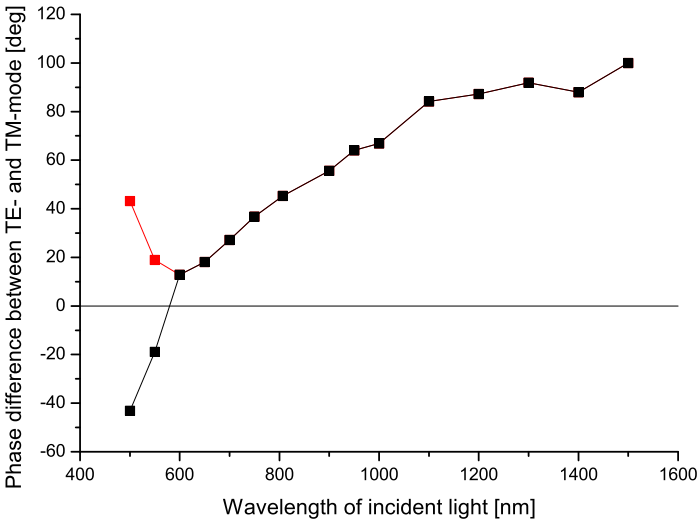

Figure 26: Fitted phase difference between modes. Because of different wave number k_z in the z-direction the modes acquire a relative phase. This leads to a more elliptical polarization. From the fit one can only get the absolute value of the phase difference, so it might flip sign below ≈ 600 nm, which gives a smoother curve. On the other hand the dielectric properties of gold change strongly below that wavelength and the phase difference might stay positive.

wavelength increases, because the polarization modes feel the difference in their boundaries conditions more strongly. The phase difference reaches a maximum of about 90 degrees in our measurements. Since the gold layer is 200 nm thick only $\approx 15\%$ of a free space wavelength fits into the length of the slit at $\lambda = 1500$ nm, giving a phase difference of maximally 50° and due to the boundary conditions the wavelength in the slit should only become longer. This means that a large part of the phase difference of 90° might come from phase jumps at the entrance or at the exit of the slit, due to impedance mismatches.

A deeper physical discussion of the results follows in Section 4.2, where I compare the measurements with the predictions of the theoretical models I derived in Section 2. This will allow us to check the validity of the model and to use it to understand the measured transmission properties of the slit (Figs. 25 and 26).

4.2 Comparison with theory

I will try to explain these results within the theoretical models that were derived earlier.

4.2.1 Waveguide

The first step is to calculate the waveguide modes for the TE- and TM-polarized component of the light. To compute the wave vectors in the slit and the transmission properties at different wavelengths I used a computer program written in *Maple*, that implements the equations from Section 2. The table of refractive indices of gold, which were used, can be found in the appendix (Table 1).
Since the equation that describes Fabry-Pérot interference (Eq. (30)) is complex, its real part can be used to determine the relative values of the TE- and TM-transmission. With the imaginary part the phase difference between the two modes can be calculated.
The slits are modeled as waveguides with a length $l = 200$ nm, which is the thickness of our gold film, and a width $a = 200$ nm. The metal structure is surrounded by air ($n_{air} = n_0 = 1$), except for the backside, where the gold is fixed on a carrier of fused quartz glass ($n_{glass} = 1.45$). Results of the calculations are shown in Fig. 27 and Fig. 28 and compared to the measured transmission properties.
All three calculation methods fail to completely explain the observed transmission characteristics of the slit. Both the calculated and the measured relative transmission decrease with increasing wavelength, but in reality the relative transmission is even higher and falls of much more slowly than the models predict. The calculations for the pure waveguide only take account of the decrease in mode-amplitude within the waveguide and neglect effects at slit entry and exit. The other calculations try to include those impedance mismatch effects by multiplying the mode-amplitude with the transmission coefficients for both slit openings (entry: air $\rightarrow$ slit, exit: slit $\rightarrow$ glass). The Fabry-Pérot-interference does not seem to raise or lower the relative transmission compared to the calculation that only simulates the impedance mismatch. For the TE-mode this is because its decay length is shorter than the slit length at most wavelengths. The undamped TM-mode on the other hand does not show Fabry-Pérot because its reflection coefficient is very small ($\approx 10\%$ of the coefficient for the transition from air to glass). To give a comparison, the modeled relative amplitude of the modes would be about a factor hundred lower if we would use the cutoff criterium $k_x = \lambda/2a$ of an ideal waveguide to determine the decay length of the TE-mode.
The pure waveguide model appears to give the correct phase difference up to a phase jump of $\approx 30°$ that might come from crossing the interfaces between air, slit and glass. At the same time both models which include the transmission coefficients fail to come even close to the observed phase difference. Why this is remains unclear, as the formulas for the Fresnel coefficients succeed in reproducing the reflectance and transmittance of, for example, glass.
Although the waveguide model certainly is an essential step towards understanding of the transmission characteristics of the metal slit apperture, it shows a surprisingly large discrepancy with the measured data. One simply cannot model the relative transmissions correctly by only looking at the waveguide behavior of the slits.

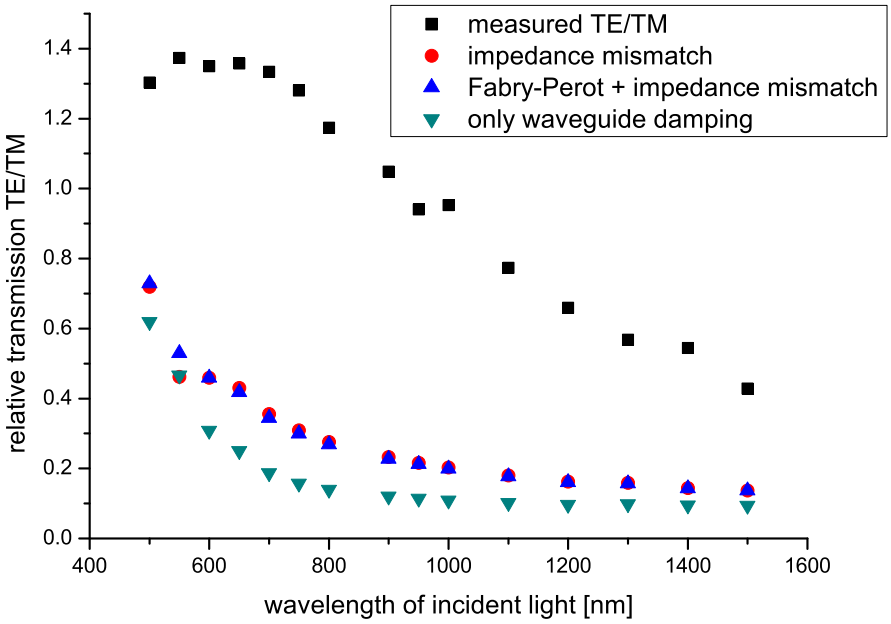

Figure 27: Comparison of the transmission amplitude that was measured with the values that were calculated with a pure waveguide model. Also plotted are the calculated values of the waveguide model with an additional impedance mismatch due to the transmission coefficients (Eq. (27)) at the slit openings with Fabry-Pérot interference as an option.

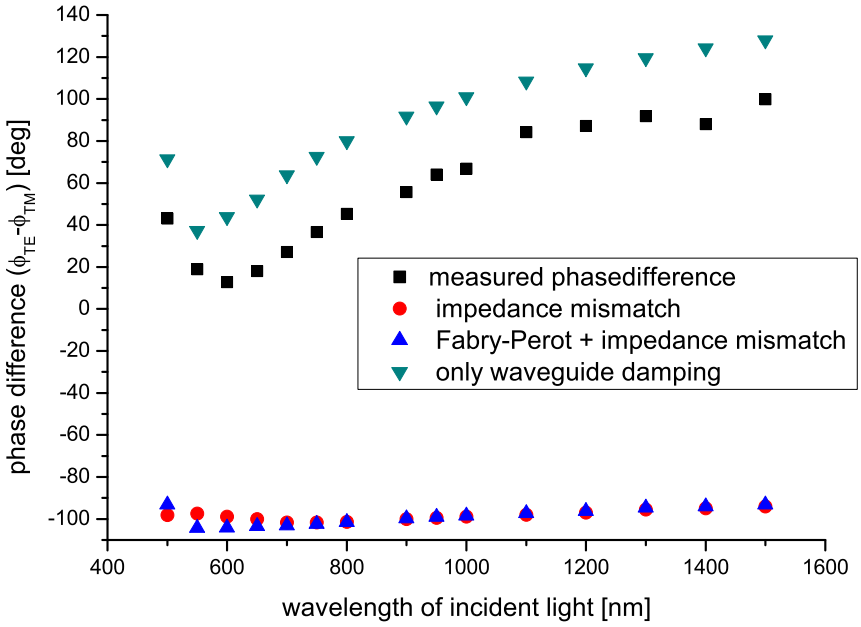

Figure 28: Comparison of the phase difference that was measured and that was calculated. The pure waveguide model reproduces the phase difference up to a shift of $\approx 30°$, which might be a result of phase shifts at the slit entry and exit. The calculations which should account for such phase shifts ("impedance mismatch") do however fail to give any useful data. It remains unclear why this is the case.

4.2.2 Plasmons

Our next goal should be to try to explain the discrepancies between the measured and calculated transmission values in Fig. 27. At this point there is no reason to believe that we underestimated transmission of TE-light significantly, so we probably overestimate the TM-polarized component. As I suggested in Section 2.4 there should be drainage of TM-amplitude due to the excitation of surface plasmons along the slit edges. The probability of plasmon excitation at a certain wavelength of incident light should be proportional to the fourier transform of the slit aperture (Eq. (32)) at a plasmon wavelength related to the wavelength of the incident light by Eq. (33).
To get the predictions of our calculation in agreement with the measured transmission data, their TM-mode would have to be weakened due to plasmon excitation by multiplication with a factor

$$f(\lambda) = \frac{TM_{meas.}}{TM_{calc.}} = (\frac{TE}{TM})_{calc.}/(\frac{TE}{TM})_{meas.}, \tag{40}$$

which can be calculated from the values displayed in Fig. 27. Figure 29 shows the result of this calculation. The graph suggest, that only about 20 to 30% of the TM-polarized light is actually entering the slits.
On the other hand we would like to see, whether this TM-weakening could be accounted for by the before mentioned plasmon excitation. Figure 30 is a graph of the function

$$\frac{H_{slit}}{H_{in}} = \sqrt{\frac{I_{slit}}{I_{in}}} = \sqrt{1 - P(\lambda)}, \tag{41}$$

which should give the reduction of the amplitude of the magnetic field of the TM-mode that enters the slit H_{slit} compared to the incident amplitude H_{in}, if the intensity I of the light is reduced to $1 - P(\lambda)$, as suggested in Section 2.4. The function $P(\lambda)$ is the plasmon excitation probability (Eq. (32)). Both graphs give the same qualitative picture, that the transmitted TM-ratio decreases with wavelength and that therefore excitation of plasmons consumes more photons at longer wavelengths. This feature supports my view, that surface plasmon excitation and the consequent weakening of the TM-mode are the main contributions to the discrepancies between the observed and calculated transmission ratio (Fig. 27). The relative agreement of the two plots has been achieved by setting the fitting parameter α to a numerical value of $2.6 \cdot 10^1 3$. This may seem like an arbitrary choice. Because the sample actually houses double-slits instead of single-slits, it is possible to get an estimate of the amount of plasmon creation by looking at the frequency spectrum of the plasmon assisted double-slit transmission, as I will explain in the following section.

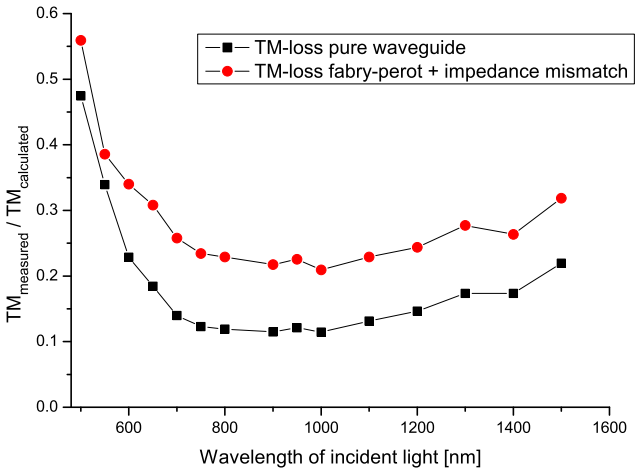

Figure 29: Dividing the relative transmission in the waveguide model by that of the actual measurements (Eq. (40)), we calculate the fraction of incident TM-polarized light that should still pass trough the slit after surface plasmons have been excited at its entrance. This is of course only correct provided that the transmission of TE is completely described by the waveguide model.

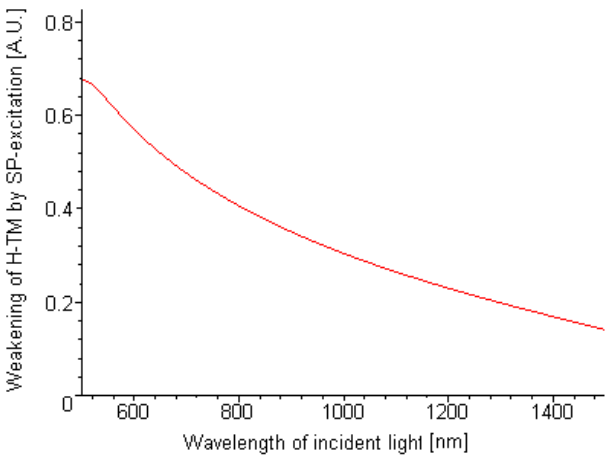

Figure 30: With Eq. (41) the amount of TM-light that is still available to travel through the slit is estimated. Because the chance of creating a plasmon is higher at a longer wavelength of the incident light, less light enters the slit. The resemblance of the wavelength dependence in Figs. 29 and 30 suggest that SPs might indeed be responsible for the discrepancies between the waveguide predictions and the actual measurements (see Fig. 27). However the factor α in Eq. (32) remains as an empirical fit parameter.

4.2.3 Plasmon mediated interference

In the double slit structures that I studied, plasmons, created at the first slit, can be converted back into light at the second slit. Part of this light will travel through the second slit and interfere with the transmission of the first slit. Because of the intermediate plasmon in the second transmission channel there will be a wavelength dependent phase difference between the two transmissions, which will produce interference fringes in a spectrogram (see Fig. 31) [2]. To investigate if the probability for plasmon excitation could be as high as I proposed in the previous section, I measured the interference of the two channels with a spectrometer (Ocean Optics SD2000).
Figure 31 illustrates how light can be transformed into plasmons and back to light, which can interfere with the directly transmitted radiation. The double-slit used for this experiment had a separation of 10 μm, with a slit-width of 200 nm. Here the transmissions of purely TM-polarized and purely TE-polarized light were measured separately by using light that is, with respect to the slit axis, polarized at an angle of 90° and 0°, respectively. The resulting spectra are shown in Fig. 32.

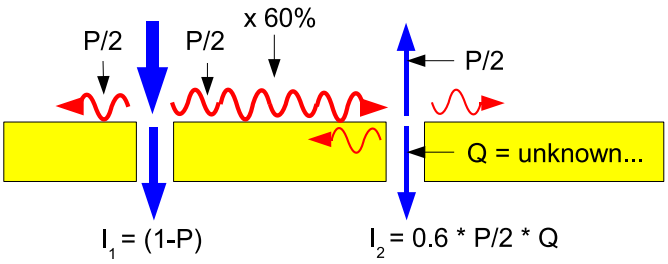

Figure 31: Plasmon assisted double-slit interference: At the first slit light is converted to plasmons with a probability P. These plasmons travel in opposite directions from the slit with equal chance. At the second slit the conversion to free space light should have the same probability. However, the probability Q of a plasmon emitting a photon into the slit is not so easily deduced, as is can also just cross the slit or be reflected at it. On the way towards the second slit a plasmon wave is damped, which can be calculated from the imaginary part of the x-component of the plasmon wave vector (see Eq. 33). For the case of a 10μm traveling distance between the slits and at a wavelength of about 700 nm for the incident light the amplitude of the plasmon wave should drop to $\approx 80\%$, resulting in a reduction of the intensity to $\approx 60\%$ of its initial value. Consequently, the light intensity I_2 at the second slit should then be $P/2 \cdot 0.6 \cdot Q$ with a relative intensity of the two interfering paths of $0.3P \cdot Q/(1-P)$.

The relative intensities of the two interfering paths (see Fig. 31) should be given by

$$\frac{I_2}{I_1} = \frac{H_2^2}{H_1^2} = \frac{0.3P \cdot Q}{1-P}. \tag{42}$$

To study the interference we would like to look at the field amplitudes of the two transmission channels instead of the measured intensity, because amplitudes can simply be added and subtracted to calculate interference effects. The conversion from intensities to field amplitudes is achieved (up to a constant factor) by taking the square root of the former.
In the measurement data for the 10μm-slit (Fig. 32) H_2 is the amplitude of the fringe oscillation around the value of H_1 in the TM-mode. The relative amplitude of these interfering magnetic fields was extracted from Fig. 32 to be $\approx 3.5/38$ at an incident wavelength of 700 nm (I assume that the relative amplitude of the two channels is constant over the range of wavelengths that constitute the fringe). Unfortunately we cannot calculate P from the ratio of the amplitudes in the two transmission channels, because there is the unknown probability Q for light to be emitted into the second slit from SPs. Still it is instructive to set Q equal P[4], for which we can calculate P to be 21%. In practice Q might even be considerably smaller than P (and consequently P would need to be larger in Eq. (42)). Of course this argumentation does not prove that TM-weakening due to plasmon excitation explains the discrepancies between the waveguide model predictions and the measured transmission, but it does show that it is not unlikely that there is a considerable amount of TM-amplitude taken away at the first slit.

[4]I made this choice for Q because I assume that the two probabilities are proportional to each other.

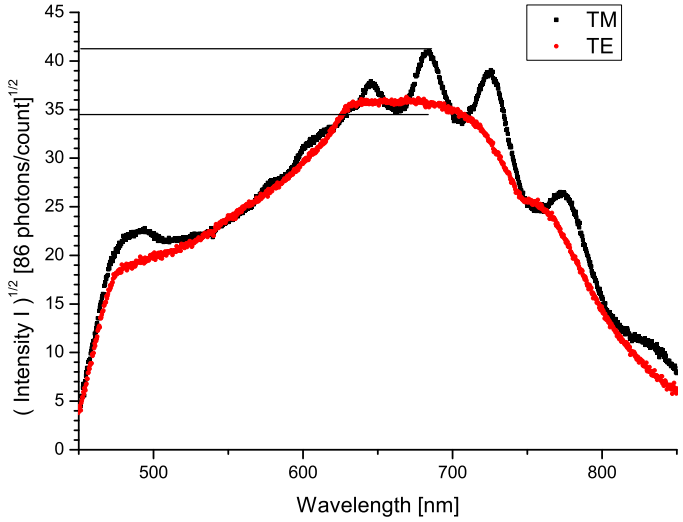

Figure 32: For a slit separation of 10μm the transmission of a double-slit was measured. To determine the relative amplitudes of the interfering fields the square root of the light intensity, which is proportional to the magnetic field amplitude of the light, is shown here. The TM-mode shows interference fringes, because in this mode plasmons are created and these produce light at the second slit that interferes with the direct transmission. The amplitude of the fringe at $\approx$ 700 nm is slightly less than 10% of the average transmission at that wavelength. The TE-modes transmission is plotted for comparison. As we would expect it does not show interference effects as there are no plasmons excited.

5 Conclusion

I have shown that a metal slit aperture has dichroic and birefringent properties that vary with the wavelength of incident light. Even far above the theoretical cutoff wavelength of the slit a considerable amount of light can pass through if the metal film in which the slit is milled is sufficiently thin. This is because the attenuation of the light depends exponentially on the length of the slit. In the slit used in the experiment the effective cutoff wavelength (given by the standing wave condition between the slit walls) turns out to be about 20% larger than the cutoff for an ideal metal slit, because in the gold film the electromagnetic fields extend slightly into the metal. At small wavelengths of the incident light the transmission for the TE-mode is measured to be higher than that of the TM-mode, which is not explained by the waveguide model. Weakening of the TM-mode due to surface plasmon excitation, might be responsible for this - a suggestion which is partially supported by the amount of TM light that is detected after being converted into a plasmon at one slit and back to light at a second slit.
Describing light transmission through a slit aperture with a pure waveguide model is not a complete model of the metal film slit transmission, one must take into account other effects like for example plasmon excitation. Still the waveguide model offers an intuitive picture of the light transmission through a metal slit. For exact numerical calculations of this transmission a finite element approach is however much more suitable and used as the standard tool (see [3, 2, 7, 9]).

6 Outlook

6.1 Future experiments

More measurements with different slit configurations and different film materials, for example silver or copper or even a dielectric, would be interesting in order to understand their transmission characteristics and to refine the proposed waveguide model. Especially a deeper theoretical analysis of the plasmon excitation seems promising to me and was unfortunately beyond the scope of this bachelor project.

6.2 Applications

Eventually I want to suggest a possible application of sub-wavelength slits in data storage media. In CDs and DVDs elongated holes, comparable to the slits in our sample, that are burned into a reflective coating are used to store digital information. The data is read by a laser beam, who's reflection from the disc is measured. Because a hole is about a quarter of the light's wavelength deep the reflected light interferes destructively with light from the surrounding material and little light is reflected. If, on the other hand, there is no hole most of the light is reflected.
I propose a CD that uses holes with slightly varying width in a thin metal film, where information is extracted from the polarization of the transmitted light. If the light would be polarized at an angle of 45° relative to the tracks of the disk, information could be stored in holes with slightly varying width. As was demonstrated in this thesis and even more so in the doctoral thesis of N.V. Kuzmin [2], the orientation of the polarization of light that passes through the slits would be very sensitive to the ratio between the width of the slit and the wavelength of the light (compare Fig. 34). Analyzing the light could for example be done, by having a number of analyzers with fixed angles and detecting which of them lets the largest intensity of the transmitted light pass through. If for example four different polarizers and hence four different width of the holes were used the storage density could become twice as big as with the current type of storage.

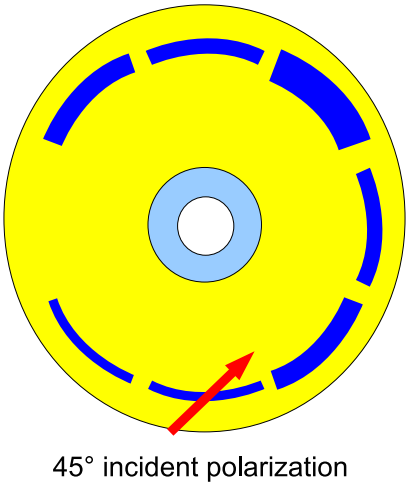

Figure 33: Datadisc with holes of different width.

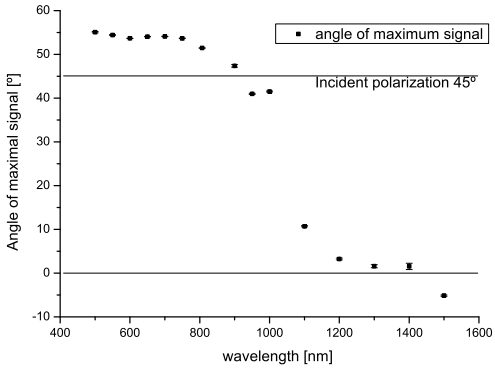

Figure 34: Small change of wavelength-to-width ratio gives large change of polarization.

7 Acknowledgements

I want to thank Eric Eliel for supervising my bachelor project. I also thank the whole group of Quantum Optics & Quantum Information for the use of their facilities, their good company and for their enthusiasm in answering my many questions.

8 Appendix

8.1 Refractive index

I give here the values of the refractive index of gold at a temperature of $25°C$ [4] for the wavelengths at which I measured:

wavelength	real index	imaginary index
500 nm	0.855	1.90
550 nm	0.359	2.69
600 nm	0.249	2.99
650 nm	0.170	3.14
700 nm	0.161	3.95
750 nm	0.169	4.58
800 nm	0.181	5.12
900 nm	0.216	6.01
950 nm	0.235	6.44
1000 nm	0.257	6.82
1100 nm	0.300	7.68
1200 nm	0.351	8.47
1300 nm	0.408	8.30
1400 nm	0.469	9.18
1500 nm	0.530	9.51

Table 1: Table of the refractive index of gold, [4].

8.2 Sample

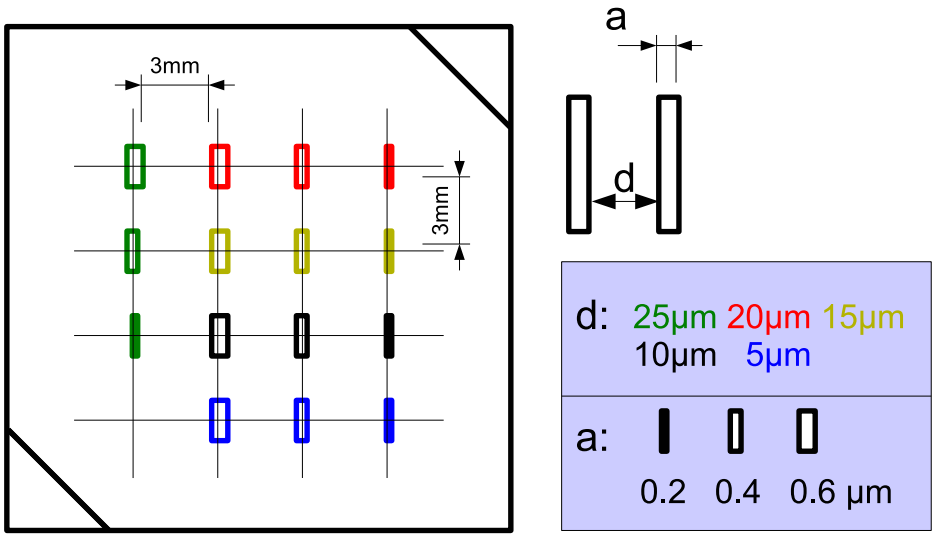

Figure 35: Slit arrangement on sample.

8.3 Components

Special attention was given to optimizing the measurement setup. Effort was put not only into improving the alignment of optical components, but also into selecting components that worked optimally at the wavelengths used in the experiment.

Light source Fianium SC-450-2 supercontinuum white light source

This source produces a wide spectrum of light with wavelengths between$\approx$ 450 nm and2000 nm with a narrow peak around 1064 nm which is the wavelength of the generating laser. The light source is operated at full power ($\approx$ 2 W) and gives a time-independent output most of the time, which is important with the measurement procedure we use. However sometimes there occur abrupt changes in the output power and measurement have to be repeated. Figure 36 shows the output spectrum of the source together with the sensitive part of our sensors for the visual/ infrared.

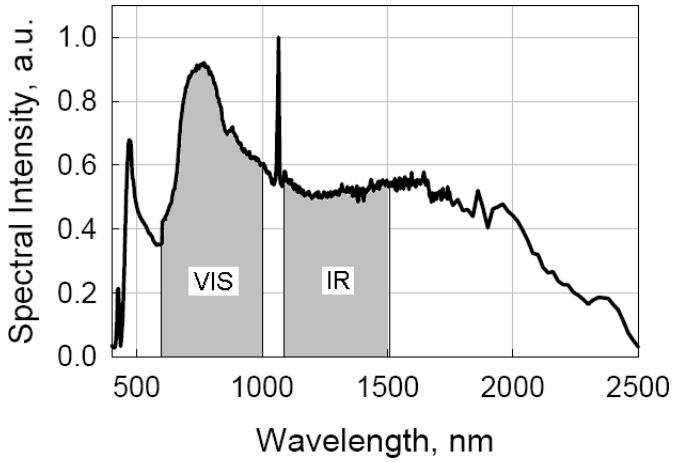

Figure 36: Spectrum of light source. Grey areas indicate sensitive region of our detectors.

Filters ThorLabs bandpass filters

To determine the wavelength dependency of the transmission a number of bandpass filters are used. The wavelengths we study are: $(500, 550, 600, 650, 700, 750) \pm 20, 800 \pm 10, 900 \pm 20, (950, 1000, 1100, 1300$ and $1500) \pm 6$ nm. The spectra for every filter were recorded both visible and infrared. It turns out, that all filters for $\lambda \leq 900$ nm also transmit a lot light in the IR above 1200 nm. Fortunately our detector for visible light does not detect light with $\lambda > 1100$ nm.

First polarizer Melles Griot 03PLS 303/A To polarize the incoming light at 45° a Glan-Laser prism with an extinction ratio of $\approx 5 \times 10^{-5}$ is used, because it works for all the wavelengths in our experiment. This was not the case for some sheet polarizers we tested. We are confident of the 45°-angle of polarization within $\pm 0.2°$.

Focus lens on sample To illuminate the sample we use a lens with focal length of 80 mm. With an estimated beam diameter of one to two millimeters the waist of the Gaussian beam would be much thinner ($\approx$ 5 μm) than the size of our double-slit configuration. Therefore the sample is put at a distance of 60 mm. The size of the light spot now is $\approx$ 1–2 mm which is a factor of 40 larger than any dimension of the double-slits. This means that the wavefront at the slits can still be seen as almost flat.

Sample The sample is mounted in a 3D-translation stage in order to be able to scroll from one double-slit to the next. An important issue is the positioning the sample. We conducted

preliminary measurements to determine the effect of the sample being tilted or the slits not being evenly illuminated. Both did reduce the quality of our measurements. By tilt we mean that the incident light does not hit the gold surface at a 90° angle. This can easily be avoided by making sure that the reflected light beam follows the path of the incident beam. If the slits are not evenly illuminated the intensity of the transmitted light drops very rapidly. So maximizing the transmission by scrolling the sample slowly under the light spot seems to be our best way of adjusting the slits.

Collimator The collimator is a stack of four lenses, its focus length was determined to be ≈ 12 mm.

Zeroth order block We use a thin metal rod to block the zeroth order of the two-slit interference pattern. This is necessary, because although the amplitude of light that just tunnels through the gold film is quite small, its contribution becomes comparable to the contribution of the two slits, when we integrate over the total size of the light spot on the sample.

Focus lens on detector To focus our light on the sensor we use a lens with a focal length of 200 mm. This length is chosen so large, because for practical reasons the analyzing polarizer is placed between the lens and the sensor. Since the polarizer works best for small angles of incidence it seems sensible to make a slowly converging beam.

Analyzing polarizer Edmund Optics - High Contrast IR sheet polarizer
The analyzer has an extinction ratio of $> 1 : 1000$ at wavelength from 650 nm to 1700 nm. This goes up to $> 10^{-5}$ around 1000 nm. At 500 nm it still seems to work quite well, so we also used it to do measurements there.
The polarizer is mounted on a rotation stage, so that the polarization axis can be turned by 360° with an accuracy of $\approx 0.2°$.

Detectors Measurements were conducted with two different detectors, both give an output voltage that is linearly proportional to the optical power striking it. The voltage is measured with a HP34401A multimeter, which can be read out by a LabView program.
New Focus NF2001: This silicon detector is sensitive to light between 400 and 1060 nm ("visible").
New Focus NF2153: The detector material is InGaAs, which has a wavelength range of 800-1700 nm ("IR"). We use this sensor instead of the NF2001 for wavelength ≥ 1100 nm.
OceanOptics SD2000 spectrometer with fiber input: We used this for a number of test measurement and to detect plasmon enhanced transmission through our sample.
Further more the OceanOptics SD4000/NIR-512 spectrometers where used to characterize our filters.

References

[1] K.E. Stubkjaer, *Technologies for Optical Processing*, Conference on Optical Fiber communication/National Fiber Optic Engineers Conference, 2008. OFC/NFOEC 2008.

[2] N.V. Kuzmin, *Interference effects with surface plasmons*, Casimir PhD Series, Delft-Leiden, 2008.

[3] O.T.A. Janssen, *Two-dimensional finite element analysis of surface plasmon effects in perforated metal films*, Master's Thesis Eindhoven University of Technology, 2006.

[4] E.D. Palik, *Handbook of Optical Constants of Solids*, Academic Press, New York, 1985.

[5] F.L. Pedrotti, L.S. Pedrotti, *Introduction to Optics*, Prentice-Hall, 1993.

[6] D.J. Griffiths, *Introduction to Electrodynamics*, Prentice Hall, 1999.

[7] C.M. Wang et al., *Transmission enhancement through a metallic slit assisted by low scattering loss corrugations*, Optics Communications, **281**, 2996 (2008).

[8] F. López-Tejeira et al., *Modulation of surface plasmon coupling-in by one-dimensional surface corrugation*, New Journal of Physics **10** (2008) 033035.

[9] L. Lalanne et al., *Approximate model for surface-plasmon generation at slit apertures*, J. Opt. Soc. Am. A **23**, 1608 (2006).